Bioactive Materials 6 (2021) 2231–2249

Contents lists available at ScienceDirect

Bioactive Materials

journal homepage: www.sciencedirect.com/journal/bioactive-materials

Transplantation of engineered exosomes derived from bone marrow mesenchymal stromal cells ameliorate diabetic peripheral neuropathy under electrical stimulation

Anamika Singh [a], Alok Raghav [a], Parvaiz Ahmad Shiekh [a], Ashok Kumar [a,b,c,*]

[a] Biomaterial and Tissue Engineering Group, Department of Biological Sciences and Bioengineering, Indian Institute of Technology Kanpur, Kanpur, 208016, UP, India
[b] Centre for Nanosciences, Indian Institute of Technology Kanpur, Kanpur, 208016, UP, India
[c] Centre for Environmental Sciences and Engineering, Indian Institute of Technology Kanpur, Kanpur, 208016, UP, India

ARTICLE INFO

Keywords:
Exosomes
Bone marrow mesenchymal stromal cells
Polypyrrole
Diabetes mellitus
Diabetic peripheral neuropathy

ABSTRACT

Diabetic peripheral neuropathy (DPN) is a long-term complication associated with nerve dysfunction and uncontrolled hyperglycemia. In spite of new drug discoveries, development of effective therapy is much needed to cure DPN. Here, we have developed a combinatorial approach to provide biochemical and electrical cues, considered to be important for nerve regeneration. Exosomes derived from bone marrow mesenchymal stromal cells (BMSCs) were fused with polypyrrole nanoparticles (PpyNps) containing liposomes to deliver both the cues in a single delivery vehicle. We developed DPN rat model and injected intramuscularly the fused exosomal system to understand its long-term therapeutic effect. We found that the fused system along with electrical stimulation normalized the nerve conduction velocity (57.60 ± 0.45 m/s) and compound muscle action potential (16.96 ± 0.73 mV) similar to healthy control (58.53 ± 1.10 m/s; 18.19 ± 1.45 mV). Gastrocnemius muscle morphology, muscle mass, and integrity were recovered after treatment. Interestingly, we also observed paracrine effect of delivered exosomes in controlling hyperglycemia and loss in body weight and also showed attenuation of damage to the tissues such as the pancreas, kidney, and liver. This work provides a promising effective treatment and also contribute cutting edge therapeutic approach for the treatment of DPN.

1. Introduction

Diabetic neuropathies (DN) are predominant and prevalent complications of diabetes mellitus (DM). This heterogeneous class presents diverse clinical manifestations affecting the nervous system. The increasing number of patients of both type 1 (T1DM) and type 2 (T2DM) diabetes mellitus is likely to contribute towards an increased number of diabetes-associated complications. Diabetic peripheral neuropathy (DPN) is a common disorder with prevalence rates of 10–26% in the adult population with DM [1]. DPN is associated with hyperglycemia-induced damage to nerve cells *per se* and neuronal ischemia due to decreased neurovascular flow resulting from hyperglycemia. Pathophysiology of DPN reveals the degeneration of nerve fibers, axonal loss, endoneurial microangiopathy, and myelin proteins degradation as key components [2]. Hyperglycemia exacerbates peripheral nerve damage by several biochemical mechanisms, including the polyol pathway, hexosamine pathway, advanced glycation end-product pathway, protein-kinase C pathway, and oxidative stress [2]. DPN is also characterized by a reduction in nerve conduction velocity (NCV) with abnormal arterioles vasodilation [3]. At present, there is no effective treatment strategy for DPN. Even glycemic control post pancreas transplantation has shown a moderate effect in regenerating the injured nerves in DPN. It is challenging to regenerate the nerve fibers and achieve functionality after neuropathy. Different therapeutic and regenerative cues such as biochemical, electrical, topographical, and cell-based cues play an important role in supporting nerve regeneration after injury [4,5]. Previously, cell-based therapy attracted much attention in DPN. Bone marrow-derived mesenchymal stromal cells (BMSCs) have shown an essential role in supporting angiogenesis and myelination of the nerves affected due to diabetes [6]. But the stem cell-based therapy comes across many practical issues such as immune-modulations, cell viability, cell apoptosis, inflammation, and

Peer review under responsibility of KeAi Communications Co., Ltd.
* Corresponding author. Department of Biological Sciences and Bioengineering, Indian Institute of Technology Kanpur, Kanpur, 208016, U.P, India.
E-mail address: ashokkum@iitk.ac.in (A. Kumar).

https://doi.org/10.1016/j.bioactmat.2021.01.008
Received 21 September 2020; Received in revised form 23 December 2020; Accepted 8 January 2021
Available online 22 January 2021

limited bioavailability, encouraging the search for a new alternate cell-free therapy. It has recently been shown that BMSCs exert their regenerative and therapeutic effect by releasing various extracellular vesicles (EVs), which transfer the genetic information and exercise their biological effect on the neighboring and distant, damaged cells or tissues through paracrine signaling [7,8].

Exosomes, a subclass of EVs, are membranous secretory nanovesicles containing biologically active proteins, lipids, nucleic acids, mRNA, miRNA, and non-coding RNAs, meant for intercellular communication with a role in various biological processes [9,10]. These nanovesicles of endocytic origin are formed in endosomal multivesicular vicinity with a diameter of 50–200 nm and secreted after fusion with the cell membrane [11]. Earlier thought to be merely cellular trash, these nano entities have been extensively explored in the last decade. It has been shown that these nano entities imitate the phenotype of the parent cell and, thus, can be analyzed for promising cell-free therapy [12]. Exosomes have been exploited as novel nanocarriers enveloped with unique attractions of abundant and non-invasive liquid biopsies. Exosomes have pragmatically delivered intercellular messages in various physiological and pathological states. Further, due to their biocompatibility, bioavailability, ability to cross the blood-brain barrier, exosomes exhibit significant carrier properties. Versatile characteristics of these nanovesicles enable researchers to load a desired cargo of interest and to produce designer engineered exosomes using surface modification methods.

BMSCs derived exosomes contain more than 150 different miRNAs and several proteins showing paracrine effects on target cells [13]. BMSCs exosomes derived from humans and rodents also showed therapeutic potential in injury models, regeneration, and neuroprotection by cargo mediated paracrine effects [14,15]. As a biochemical cue, these exosomes have shown repair and regeneration of injured nerve, bone, cardiac, and liver tissues [16,17]. Previously, we have demonstrated the role of exosomes laden wound dressing OxOBand, in alleviating diabetic wound healing [18]. OxOBand, oxygen releasing antioxidant polyurethane cryogels based dressing supplemented with Adipose-derived stem cells (ADSCs) exosomes promoted diabetic and infectious wound healing. Due to hyperglycemia, oxidative stress, and reactive oxygen species (ROS) are generated. The exosomes are nanovesicles with enriched cargo that can combat the oxidative stress and ROS [18,19]. The therapeutic and regenerative potential of exosomes is seemingly boundless, opening hope in DPN. Earlier, MSCs derived exosomes have shown a therapeutic effect in the treatment of T1DM and T2DM [20–22]. In T1DM rats, the treatment of BMSCs derived exosomes showed improvement in the blood glucose and plasma insulin levels. BMSC exosomes treatment also increased pancreatic beta islets in number and size and enhanced upregulation of pancreatic tissue genes such as Pdx1, Smad2, Smad3, and TGF-β, demonstrating the regenerative effect of the exosomes as compared to the BMSCs and diabetic control [22]. Intraperitoneal delivery of ADSC derived exosomes regenerated the pancreatic beta islets producing insulin in the T1DM mice model [20]. Mesenchymal stem cells derived exosomes alleviated T2DM by decreasing the blood glucose levels, controlling beta-cell apoptosis, and increasing insulin sensitivity [23].

For alleviating neuropathy, another cue which could play an essential role in nerve repair and regeneration is the electrical conductivity [24,25]. Nerves, as already known, are conducting entities carrying vital signals. Besides repairing at a cellular level, it is also mandatory to restore the conduction property of nerves lost due to DPN. Electrically conducting material and electrical stimulation (ES) will provide a guidance cue in enhancing the myelination and regeneration of the damaged axons after injury. Electrical stimulation relieves neuropathic pain and enhances nerve regeneration after DPN by increasing the expression of growth factors like VEGF and NGF, thus improving angiogenesis and reducing inflammatory markers [26]. Electrical stimulation has been used as a therapeutic strategy; however, no system has successfully provided high selectivity and efficacy. Therefore, for efficient delivery of current at the targeted site, conductive polymers are used along with electrical stimulation (ES). Thus lower stimulus is required for generating the same or more regenerative outcome [27]. Therefore, it will also be interesting to look into the effect of conducting system in combination with ES in DPN. Under ES, the conducting polymers enhance cell adhesion, differentiation, and DNA synthesis in electrically responsive cells [28]. Polypyrrole is an electrically conducting polymer that is enormously explored for both in-vitro and in-vivo nerve regeneration [29–31]. Along with its excellent redox activity, it is biocompatible and possesses antioxidant properties [32]. ES through polypyrrole based biomaterials has increased neurite outgrowth in the nerve cells [33,34]. For combining both the cues into a single entity, a delivery vehicle or a carrier is required. As an advanced nano delivery vehicle, liposomes are well established for carrying biologically active compounds for various applications. Previously, liposomes were fused with exosomes to deliver large size DNA plasmids [35]. Thus, to fabricate a designer conducting exosomal system (DCES), an imperative approach will be to fuse exosomes with polypyrrole nanoparticles (PpyNps) containing liposomes.

Therefore, for the treatment and management of DPN, in the current study, we envisaged developing a multifaceted approach where biochemical cues in the form of exosomes and biophysical cues in the form of electrically conducting PpyNps along with exogenous electrical stimulation will lead to nerve repair and regeneration. We hypothesized that biochemical cues would ameliorate nerve regeneration after DPN, and the electrical cues would work synergistically to enhance the regenerative outcome. To serve this purpose, we engineered the required system by following these sequential steps; (1) exosome biogenesis from BMSCs, (2) synthesis of PpyNps, (3) packaging of PpyNps into liposomes, and (4) fusion of exosomes and packed liposomes. The conducting cargo containing exosomes along with ES was delivered to the damaged nerves and evaluated for providing therapeutic effects in DPN. The developed DCES was characterized for its physicochemical properties, investigated in in-vitro studies, and finally challenged its therapeutic potential in an in-vivo DPN model.

2. Results and discussion

2.1. Isolation and characterization of BMSCs exosomes

The exosomes were isolated from mesenchymal stromal cells derived from bone marrow as represented in the scheme in Fig. 1A and quantified for total protein by bicinchoninic acid (BCA) assay. As determined, the total protein concentration was 900 ± 142.24 μg/mL. The isolated exosomes analyzed in field emission scanning electron microscopy (FE-SEM) revealed non-agglomerated and spherical morphology **(Fig. 1 (B1))**. The transmission electron microscopy (TEM) image revealed that the BMSCs exosomes have characteristic lipid bilayer membrane and cup-shaped morphology **(Fig. 1 (B2))**. The Cryo-EM imaging of the exosomes revealed the distinctive round shape **(Fig. 1 (B3))**. The size of the exosomes in the TEM image **(Fig. 1 (B2)** was less than the Cryo-EM image **(Fig. 1 (B3)),** which could happen due to the drying effect of the exosomes in TEM imaging. However, in Cryo-EM, the exosomes were visualized without drying or desiccation. The exosomes were detected and visualized using confocal fluorescence microscopy. As exosomes are lipid vesicles, therefore they showed labeling with PKH-26 dye, which incorporates through its long aliphatic tails into the lipid membranes. The PKH-26 (red color) labeled exosomes were observed in the confocal fluorescence image **(Fig. 1 (B4))**. To further analyze the hydrodynamic diameter and concentration of the exosomes, nanoparticle tracking analysis (NTA) was performed. The size of the isolated BMSCs exosomes, according to NTA, was 211.8 ± 76.5 nm **(Fig. 1 (B5))** with a predicted concentration of the exosome particles as 4.72×10^8 particles/mL. Concerning protein concentration, the exosome concentration was 1.88×10^8 particles/μg of protein. The presence of the exosomes was also analyzed by immunogold labeling for the CD-9 surface marker. The TEM micrograph shows the presence of the immunogold labeled exosomes

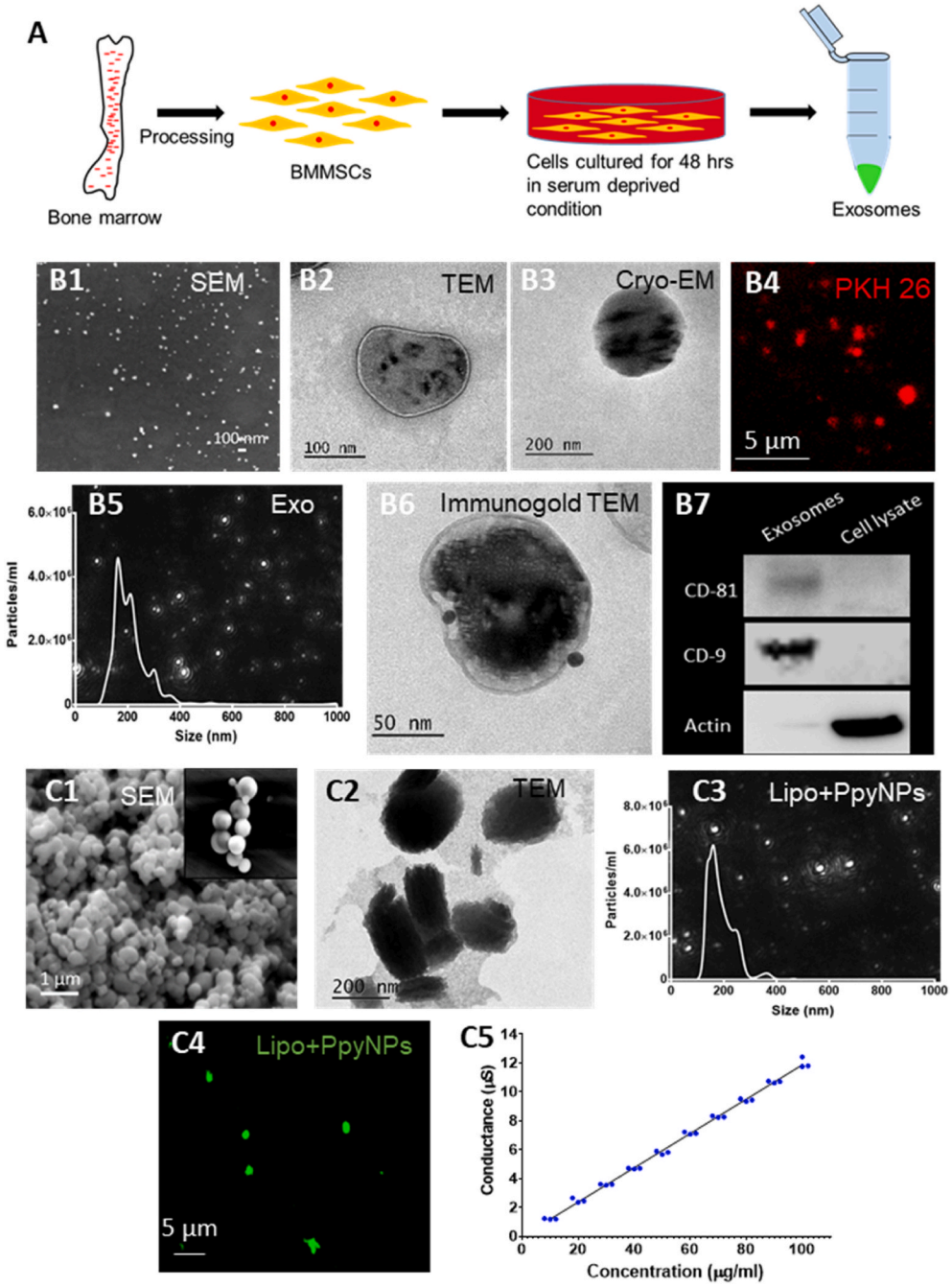

Fig. 1. (A) Scheme represents the isolation of exosomes from rat bone marrow-derived mesenchymal stromal cells. BMSCs exosome characterization (B1) FESEM micrograph of BMSCs derived exosomes showing uniformly distributed and non-agglomerated particles, (B2) TEM image of exosomes showing bilayered lipid vesicles, (B3) Cryo-EM image of the exosomes, (B4) confocal fluorescence microscopic image representing exosomes labeled with PKH-26 dye, (B5) Nanoparticle tracking analysis, (B6) TEM micrograph illustrating immunogold labeling of CD9 marker on exosomes, and (B7) western blotting analysis of exosomes for CD-81, CD-9, and actin expression. (C1) FESEM micrograph of polypyrrole nanoparticles (PpyNps) formed by chemical oxidation and reduction method (inset showing particles with fine zoom), (C2) TEM micrograph of liposomes, (C3) Nanoparticle tracking analysis of polypyrrole nanoparticles containing liposomes, (C4) confocal fluorescence microscopic image representing polypyrrole nanoparticles containing liposomes labeled with PKH-67 dye, and (C5) measurement of the electrical conductance of PpyNps at different concentrations ranging from 10 to 100 µg/mL.

with anti-CD-9 antibody **(Fig. 1 (B6))**.

Further, the exosomes were characterized by western blotting for the specific exosomal markers. The presence of endosomal expression of CD81 and CD9 in the western blotting confirmed the presence of exosomes **(Fig. 1 (B7))**. As expected, these markers were not expressed in the cell lysate, where actin expression was observed.

2.2. Preparation and characterization of PpyNps, liposomes, and fused exosomal system

Polypyrrole nanoparticles (PpyNps) were synthesized by a chemical oxidation polymerization reaction [36]. Cationic iron present in the ferric chloride acted as the oxidizing agent to initiate the polypyrrole monomer's chemical oxidation reaction to form PpyNps. As observed in the FE-SEM image, the synthesized PpyNps were spherical in morphology **(Fig. 1 (C1))**. As determined by DLS, the average size of the PpyNps was 88.40 ± 3.46 nm. As a vehicle for incorporating PpyNps, liposomes were prepared using the thin-film hydration method. Cationic liposomes are associated with certain drawbacks related to in-vitro and in-vivo cytotoxicity and may not be used for the delivery approach [37]. Therefore, in the present study, anionic liposomes were prepared that may be preferred for the delivery of the nanoparticle's cargo into cells [38]. TEM images of the synthesized liposomes indicated the near-circular type morphology and nano dimensions **(Fig. 1 (C2))**. Anionic liposomes showed slower release kinetics of clearance. They helped to extravagate the cargo inside, better serve our purpose of delivering the cargo effectively and efficiently to the cells for performing therapeutic action [38]. Anionic liposomes have a better association with the cell membrane that allows its fusion and also overcome the barriers of cytotoxicity and instability associated with cationic

liposomes. However, the mechanism behind their effectiveness in cellular delivery is unclear. The liposome to cell interaction depends on various factors, including the cell type, charge density, and lipid head group. Their uptake may occur when the cell to liposome charge ratio achieves a certain fixed threshold [39,40].

The size of the liposomes, as measured in NTA, was 189 ± 51.9 nm (**Fig. 1 (C3)**). The liposomes were also detected and visualized by fluorescence microscopy. The lipid membrane of the liposomes showed binding to the PKH-67 dye (green color), as observed in the confocal fluorescence image (**Fig. 1 (C4)**). Before the incorporation of the PpyNps into liposomes, the PpyNps were characterized for the electrical conductivity. Polypyrrole (Ppy) has suitable conduction property and environmental stability [41]. The electrical conductance of PpyNps was measured at different concentrations (**Fig. 1 (C5)**). The smaller PpyNps contribute to high surface area attracting higher electron charge density at the surface, thereby allowing higher electron motion. We observed an increase in the conductance with subsequent increase in the concentration of the PpyNps.

To incorporate the biochemical cues and electrical cues in a single entity to develop the designer conducting exosomal system, the BMSCs derived exosomes were fused with the PpyNps containing liposomes using a freeze-thaw method as represented in Fig. 2A [42]. The fusion of

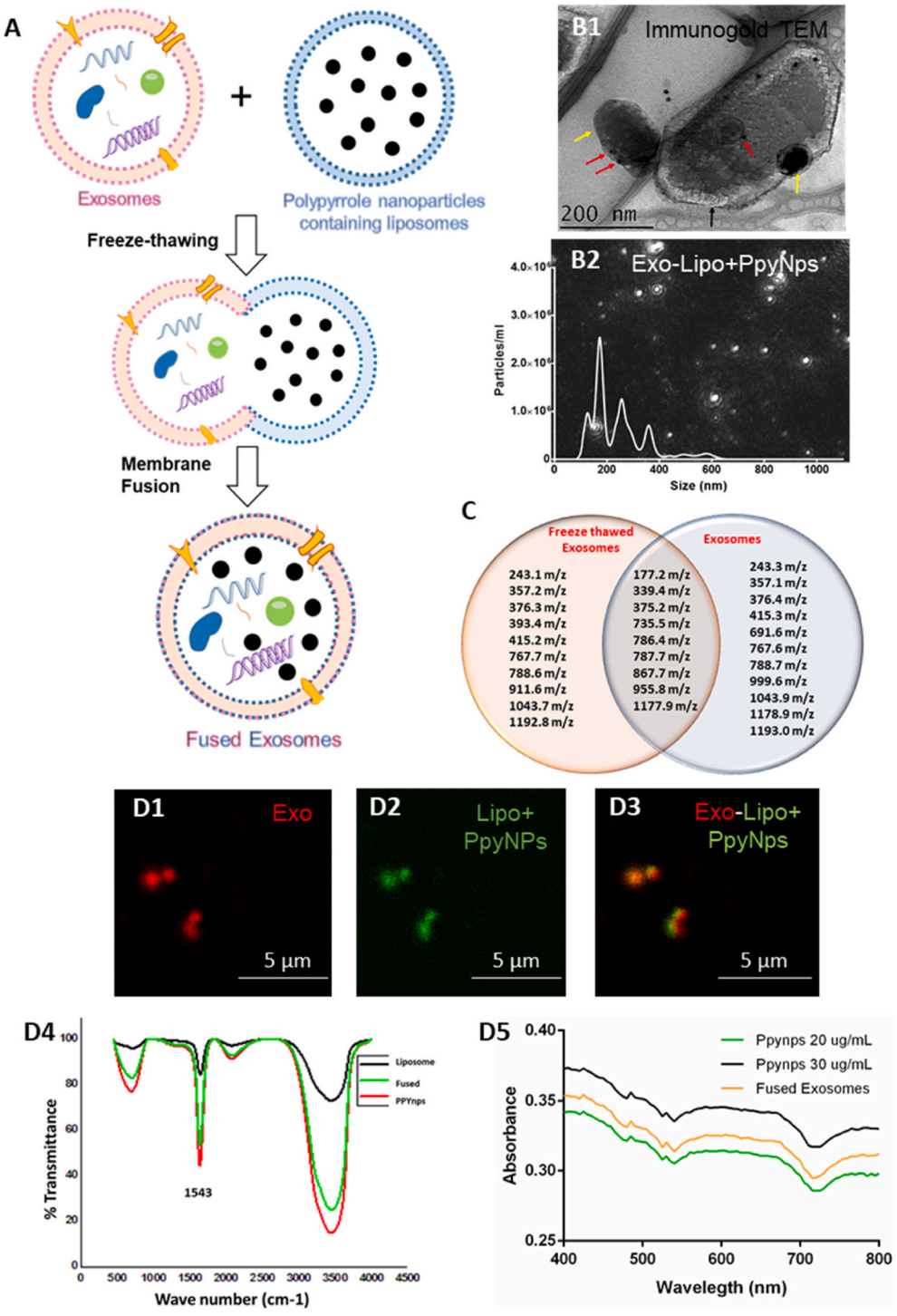

Fig. 2. (A) Scheme representing membrane fusion of exosomes and PpyNps containing liposomes by the freeze-thawing mechanism. Analysis and characterization of the fusion between liposomes and exosomes, (B1) TEM micrograph of fused exosomes and liposomes, where the yellow arrow indicates exosome, black arrow shows liposome, and the red arrow indicates gold nanoparticles bound to CD-9 exosomal marker, (B2) Nanoparticle tracking analysis of exosomes fused with polypyrrole containing liposomes. (C) Venn diagram representing numbers of mass peaks detected in LC-MS data of the freeze-thawed exosomes and normal exosomes. Confocal fluorescence microscopic analysis representing (D1) exosomes labeled with PKH-26 dye, (D2) Polypyrrole nanoparticles containing liposomes labeled with PKH-67 dye, (D3) fusion of liposomes and exosomes, (D4) Infrared spectra of PpyNps showing vibrations at 1543 cm-1 after incorporation into liposomes thereby confirming its presence into liposomes, (D5) UV spectra absorption profile of PpyNps at different concentrations, PpyNps containing liposomes, and also after fusion with exosomes, thereby showing the shoulder effect which is a peculiar feature of PpyNps

membranes containing lipid-rich niches (i.e., liposomes and exosomes) involves the transition of multi-lamellar liposomes into single hefty uni-lamellar liposomes with the incorporation of water-soluble content within the water phase of liposomes, suggestive of membrane disruption and ice-crystal formation [42]. The extent of fusion between the exosomes and liposomes vesicles was determined by fluorescence self-quenching R18 assay. The R18 binds to the liposomes lipid membrane, and at a particular concentration, it shows self-quenching of the fluorescence due to dye-dye interaction. We observed that for the labeling of liposomes membrane, 3.5 μl of the dye was sufficient and showed maximum self-quenching. After fusion, the distance between the dye molecules increases, leading to an increase in fluorescence. We quantified the increase in fluorescence and obtained a fusion efficiency of 28% between the liposomes and exosomes. Our results are in corroboration with the earlier study on the fusion between the extracellular vesicles and liposomes [43]. The unfused exosomes and polypyrrole nanoparticles containing liposomes were not separated from the fused product after the fusion process. Both are functional entities to deliver cues to the cells. Liposomes carry conducting particle, which they could deliver to the cells and enhance conductivity. It was attempted to separate the unfused particles using a gel filtration technique and density gradient centrifugation; however, it did not work due to technical limitations like similar size ranges and loss of the yield. The TEM micrograph also demonstrated the fusion of the exosomes with liposomes after freeze-thawing **(Fig. 2 (B1))**. The exosomes lipid membrane fuses with the liposomes membrane in the membrane deformation and reformation process during the freeze-thawing process. The presence of the exosomes in the fused product was further analyzed by the immunogold labeling for the CD-9 exosomal marker, which confirmed the fusion of liposomes with exosomes. The size and concentration of the fused-Exo particles were 247 ± 120.3 nm and 2.48 × 10^8 particles/mL, according to NTA **(Fig. 2 (B2))**.

To analyze that the freeze-thawing process has not ruptured the exosomal membrane, we did LC-MS analysis of the normal exosomes and freeze-thawed exosomes. The MS spectra of the exosomes before and after freeze-thawing are represented in Fig. S1. The freeze-thawed exosomes didn't show significant changes in m/z peaks compared to normal exosomes. The Venn diagram **(Fig. 2C)** showed typical peaks present at the intersection, indicating that the freeze-thaw technique of modifying exosomes didn't significantly contribute to any changes in the protein contents. The immunogold labeling of the freeze-thawed exosomes also revealed that the vesicles have intact membrane and preserved surface markers, as observed in the TEM micrograph **(**Fig. S2 (A)**),** which is important for being functionally active. Further, Calcein-AM fluorescence imaging, which depends on the esterase activity of the exosome contents, also confirmed that the freeze-thawed exosomes are functional and not ruptured (Fig. S2 (B)). Thus, the freeze-thaw approach has not affected the integrity and peptide content of the exosomes used in DPN therapy. The fusion of exosomes and PpyNps containing liposomes was also observed through fluorescence microscopy imaging **(Fig. 2 (D1-D3)**.

The lipid membranes of the exosomes and liposomes were labeled with PKH dyes, i.e., PKH-26 (red color) and PKH-67 (green color), respectively, and were observed in the confocal fluorescence microscope after fusion. The merged image showed the co-localization of the red and green fluorescence indicating the fusion of exosomes and liposomes lipid vesicles, respectively **(Fig. 2 (D3))**. Here, the liposomes and exosomes shown in the confocal fluorescence images do not represent the vesicles actual sizes. Fourier-transform infrared spectroscopy (FTIR) analysis was done to confirm the incorporation of the PpyNps in the liposomes and fused-exosomes. FTIR analysis of the PpyNps showed the characteristic peak at 1543 cm^{-1} that corresponds to the polypyrrole ring vibrations **(Fig. 2 (D4)**. A similar peak was observed for PpyNps containing liposomes and Fused-Exo, showing the incorporation of the PpyNps [44]. The UV–Visible spectroscopy also confirmed the incorporation of the PpyNps in the PpyNps containing liposomes fused with exosomes (Fused-Exo) **(Fig. 2 (D5))**. The absorption band at 430 nm was attributed to the π-π* transition of polypyrrole chains with different oxidation levels, while the absorption at 460 nm corresponds to the pyrrole oligomer. Moreover, the π-π* transition of polypyrrole ring presents "shoulder effect" at λ∼448 nm, further not altered after incorporation into liposomes and fusion with exosomes [36]. The band with broad-spectrum characteristics at 750 nm denotes transitions from the valence band into the bipolaron band, which indicates polypyrrole doping [45]. To estimate the cellular metabolic activity in the presence of PpyNps, liposomes, and PpyNps containing liposomes, MTT assay was performed. The data showed that metabolic activity increased with time in the presence of the synthesized material **(Fig. S2 (C–E))**. In the present study, DCES offers a novel strategy for using it as a nanocarrier delivery system carrying conducting polymer with therapeutic and regenerative potential.

2.3. Exosomes internalization in neural cell lines and evaluation of protective effect against oxidative stress

To exert any cellular effect, the exosomes should be internalized inside the cells. There are various mechanisms described in the literature to internalize exosomes to elicit a cellular response, including endocytosis, phagocytosis, and micropinocytosis [46–48]. We investigated the internalization of PKH-26 labeled exosomes inside two different neural cell lines, SH-SY5Y and Neuro2a cells. We observed that the labeled exosomes started internalizing in SH-SY5Y cells after 1 h of incubation in the live-cell confocal fluorescence microscopy **(**Fig. 3 **(A1))**. Further, we detected an increased uptake of exosomes in the cells with time observed for a period of 12 h **(Fig. 3 (A2-A3))**. To analyze that the isolated exosomes have intact vesicles and are not lysed or permeabilized, Calcein-AM staining was performed. Calcein-AM dye is hydrophobic, non-fluorescent, and permeable to the cell membrane. Upon interacting with the esterases present within the vesicles, the dye is hydrolyzed to give Calcein-AM, which shows fluorescence and is impermeable [49]. We observed the internalization of Calcein-AM labeled exosomes inside the SH-SY5Y cells **(Fig. 3 (A4))**. The results showed that the isolated exosomes from BMSCs are true intact vesicles, which is important for being functionally active. The orthogonal confocal microscopic image shows that the Calcein-AM labeled exosomes are internalized in the cells and are not attached to the cell surface **(Fig. 3 (A5))**. We also observed the internalization of PKH-26 labeled exosomes in Neuro2a cells **(Fig. 3 (B1–B3)**. Cells were efficiently internalized by Neuro2a cells similar to that of SH-SY5Y cells. Also, the Calcein-AM labeled intact exosomes were internalized inside the Neuro2a cells after incubation, as observed in the live-cell imaging **(SV1).** Freeze thawing can change the structural morphology to affect exosome internalization. So, we also studied the internalization of the fused exosomes and liposomes developed by the freeze-thawing process in SH-SY5Y cells. The fused exosomes were also internalized inside the SH-SY5Y cells similarly to naive exosomes as represented in the confocal microscopic images **(Fig. 3 (C1–C3))**. Further, we quantified the fluorescence intensity of the internalized exosomes and fused-exosomes inside the SH-SY5Y cells **(Fig. 3 (D))**. The total fluorescence intensity measured per unit area was similar before and after fusion, which demonstrates that the fusion process has not affected the internalization of the exosomes inside the cells.

To investigate the protective effect of exosomes against oxidative stress, we used two different in-vitro models. SH-SY5Y cells were cultured in high-glucose media (150 mM) to induce glucose toxicity. The SH-SY5Y cells were used for the toxicity analysis as it is the most extensively used neuroblastoma cell line to study diabetic neuropathy in in-vitro conditions. These cells show similar results to primary dorsal root ganglion neurons and Schwann cells in high glucose conditions, as reported earlier [50]. High glucose toxicity leads to the generation of reactive oxygen species (ROS) *via* multiple mitochondrial and non-mitochondrial pathways. High glucose toxicity also causes damage to DNA, lipids, proteins and confers neurotoxicity. ADSC exosomes have

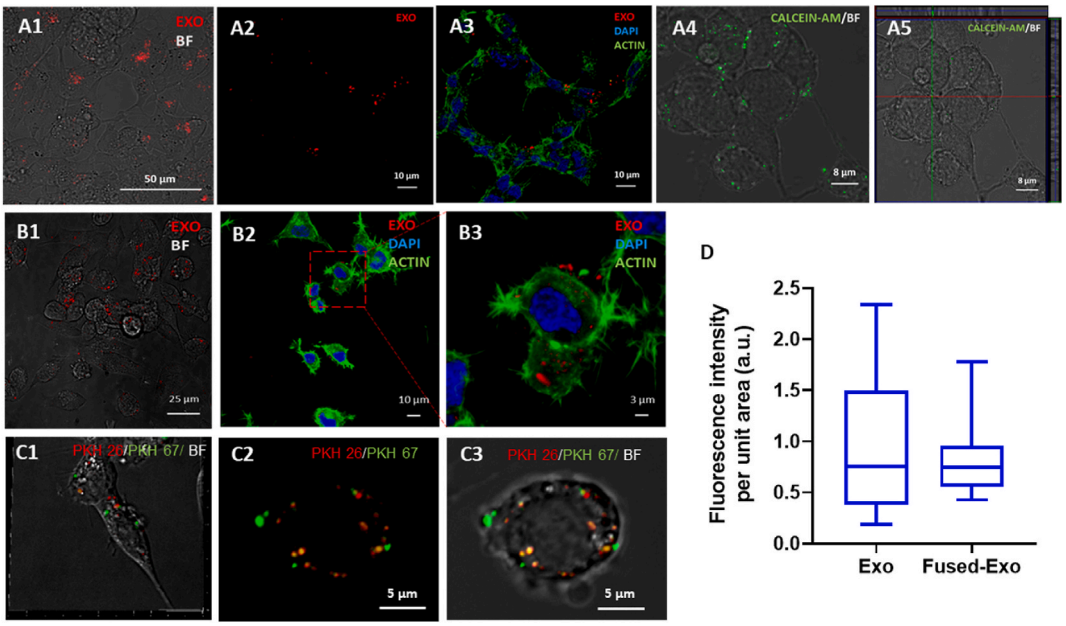

Fig. 3. Internalization of BMSCs-Exo and fused-Exo in neural cell lines. (A1) PKH-26 labeled exosomes (red) internalized into SH-SY5Y cells after 1 h of incubation as represented in fluorescence and bright field merged image, (A2-A3) The internalization enhanced with time and observed maximum after 12 h of incubation as illustrated in the FITC/DAPI (green/blue) labeled cells representing exosomes (red), (A4) Calcein-AM labeled BMSCs-Exo representing intact exosomal vesicles internalized inside SH-SY5Y cells, (A5) the orthogonal view of the internalized exosomes represents its internalization inside the cell. Confocal fluorescence images representing internalization of exosomes in Neuro2a cells (B1) PKH26 labeled exosomes (red) inside Neuro2a cells, (B2) FITC/DAPI (green/blue) labeled cells representing exosomes (red) internalization, (B3) High resolution magnified image of (B2) representing exosomes internalized inside Neuro2a cells. Confocal fluorescence image representing internalization of fused exosomes and liposomes (C1) 3D fluorescence image of fused particles internalization inside the SH-SY5Y cells. (C2–C3) Fused exosomes synthesized by fusion of PKH26 labeled exosomes (red) and PKH67 labeled liposomes (red) were internalized inside SH-SY5Y cells. (D) Measurement of the total fluorescence intensity of the exosomes and fused-exosomes internalized in the SH-SY5Y cells.

shown anti-hyperglycemic effect in SH-SY5Y cells, when supplemented to the cells at 20 μg/ml concentration [18]. Initially, we optimized two concentrations of 20 μg/ml and 30 μg/ml for the BMSCs derived exosomes. However, we did not observe any significant increase in cell viability under the hyperglycemic condition at 20 μg/ml of BMSCs exosomes (data not shown), whereas significant improvement was observed at 30 μg/ml concentration. For the toxicity studies, 30 μg/ml of exosome concentration was used. In MTT assay and live/dead imaging, we observed that exosomes treated SH-SY5Y cells were protected against cellular death as compared to non-treated cells (Fig. 4 **(A1-A2)**). Cellular viability measured in terms of live cells (%) was significantly higher in the exosomes treated group than the non-treated cells (Fig. S3 (A)). The BMSCs derived exosomes have some antioxidant components that might have protected the cells in the oxidative stress environment. Recently it has been shown that mesenchymal stem cells derived exosomes have neuroprotective and antioxidant effects on neural cells against oxidative stress generated by different molecules such as hydrogen peroxide and amyloid β-peptide [51,52]. MSCs derived exosomes contain active catalase for combating oxidative stress having profound therapeutic effect on neurodegenerative diseases [52]. Further, we evaluated the effect of exosomes in attenuating oxidative stress in Neuro2a cells using menadione, which is a neurotoxin and causes oxidative stress by the generation of ROS through redox cycling in the cells [53]. We investigated the effect of exosomes against menadione generated oxidative stress on the cellular viability and proliferation of Neuro2a cells.

Under oxidative stress, Neuro2a cells survived better in the presence of the exosomes as compared to non-treated cells. In the live/dead imaging, we observed more viability in exosomes treated cells as compared to non-treated cells after 12 h (Fig. 4 **(B1)**. Similar results were observed in the MTT assay, where the cellular metabolic activity was more in exosomes treated cells than non-treated cells (Fig. 4 **(B2)**. These results showed that BMSCs derived exosomes have neuroprotective and antioxidant properties to reduce the effect of the ROS. To ascertain that the protective effects of the exosomes are maintained in the fused product of exosomes and liposomes after freeze-thawing, we also evaluated the prosurvival effect of fused exosomes in attenuating cell death under hyperglycemia. The MTT assay and live/dead imaging showed that fused exosomes treated SH-SY5Y cells were protected against cellular death as compared to non-treated cells (Fig. 4 **(C1–C2))**. Also, the percentage of the live cells was higher in the fused exosomes treated group than the non-treated group (Fig. S3 (B)**)**. This affirmed that the fused product (DCES) has maintained its neuroprotective and antioxidant potential. DCES will inhibit the generated oxidative stress which is one of the major causes of nerve degeneration in diabetic neuropathy. We further evaluated the therapeutic effect of DCES in an in-vivo DPN model.

2.4. Fused conducting exosomal system enhanced electrophysiological parameters

To investigate the therapeutic effect of DCES, we established a rat DPN model by intraperitoneal injection of streptozotocin. Electrophysiological parameters such as motor nerve conduction velocity (MNCV) and compound muscle action potential (CMAP) decreased in STZ-induced DPN animals compared to the healthy group, recorded at sciatic-tibial nerve region. There was a 40% reduction in electrophysiological parameters indicating the development of severe DPN, 8 weeks post STZ injection. The experimental design of the in-vivo DPN study is represented in Fig. 5A. Stem cells have been investigated for the treatment of DPN, however, the translation of the therapy from bench to bed side has been difficult due to certain underlying disadvantages such as ideal route and dose of administration, concern of tumor development and low cell retention capacity [54]. Moreover, there are growing evidences that the therapeutic effect of these stem cells is due to secretion of paracrine factors such as exosomes.

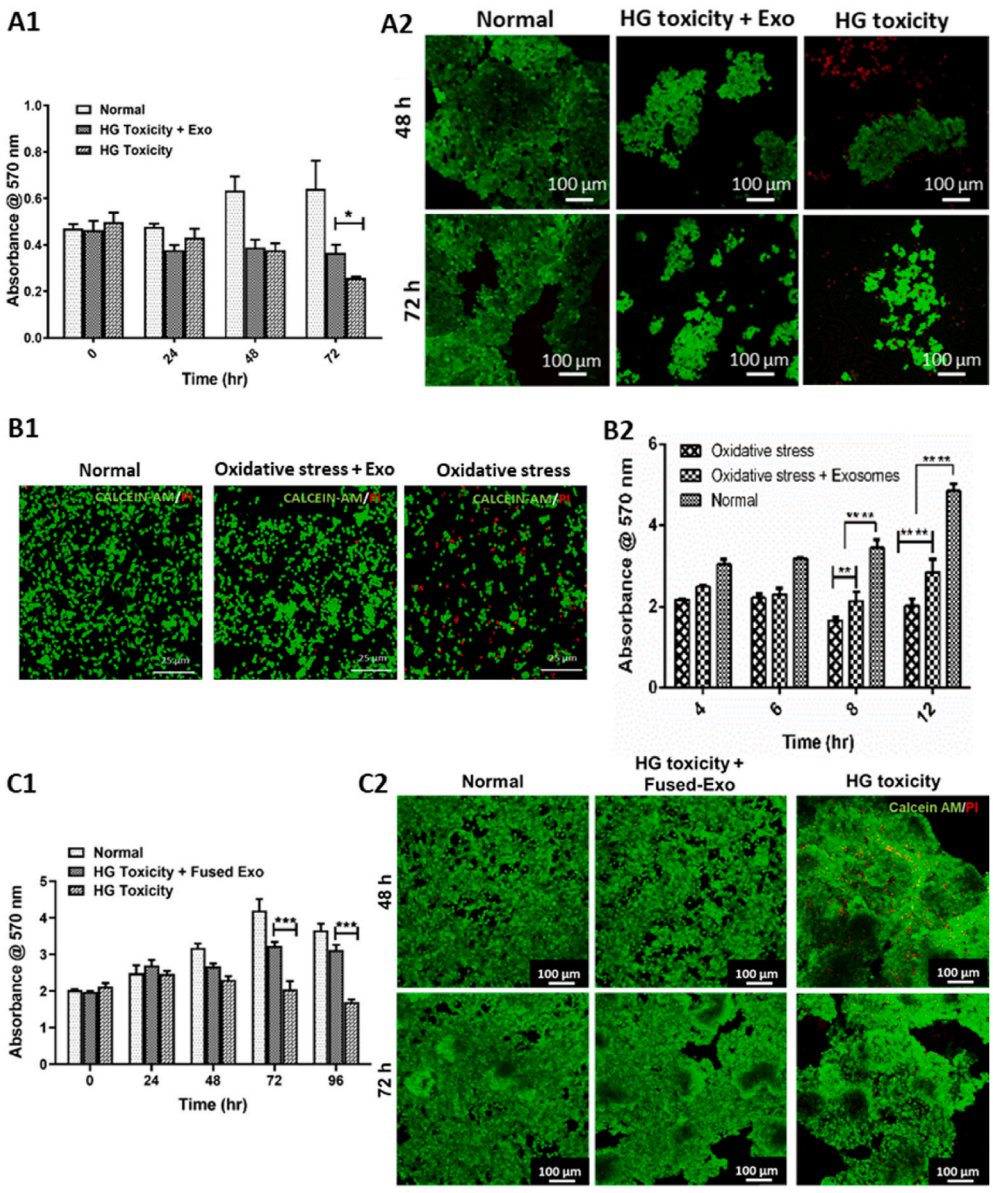

Fig. 4. BMSCs-Exo and fused-Exo enhanced neural cell viability against oxidative stress environment. BMSCs-Exo protected SH-SY5Y cells against high-glucose toxicity as represented by (A1) MTT assay, and (A2) Live/dead staining using Calcein-AM and PI, which shows more viable cells in high glucose toxic environment in the presence of exosomes. BMSCs-Exo protected Neuro2a cells against oxidative stress generated by menadione (20 μM) as represented in (B1) live/dead assay using Calcein-AM/PI and (B2) MTT assay. Fused exosomes protected SH-SY5Y cells against high-glucose toxicity as represented by (C1) MTT assay, and (C2) Live/dead staining, which shows that the freezing-thawing process during fusion of exosomes and liposomes has not ruptured the exosomes and maintained their functionality. *$p \leq 0.05$, **$p \leq 0.01$, ***$p \leq 0.001$, ****$p \leq 0.0001$.

For the amelioration of DPN, the exosomal therapy was given intramuscularly in the gastrocnemius muscle. The intramuscular administration of the exosomal therapy at the injured site is more efficient than the systemic administration due to their increased half-life index resulting in enhanced bioavailability [55]. Exosomes injected at the gastrocnemius muscle are transported to the dorsal root ganglion, and spinal cord via sciatic nerve through retrograde axoplasmic transport [56]. We evaluated the potential of the developed therapy in normalizing the nerve functionality by measuring MNCV and CMAP after 4, 6, and 8 weeks of the treatment. After 4 weeks, there was a significant improvement in electrophysiological parameters of the treated animals as compared to the negative control. The MNCV is indicative of the conductance of the nerve fibers. Our combined therapy of designer conducting exosomal system (DCES) along with electrical stimulation (ES), i.e., (Fused-Exo + ES) considerably improved the MNCV (56.57 ± 0.51 m/s vs 25.73 ± 1.16 m/s) compared to negative control group (**Fig. 5 (B1)**). We observed substantial improvement in MNCV values in Fused-Exo (49.67 ± 2.85 m/s) and Exo (48.63 ± 1.21 m/s) group as compared to the negative control, however, the effect was significantly less than the combined therapy. Also, the MNCV values in Fused-Exo + ES group (56.57 ± 0.51 m/s) were comparable to that of healthy control (60.25 ± 1.56 m/s). These results demonstrated the combined effect of the fused exosomes along with electrical stimulation in enhancing MNCV, and thus nerve regeneration.

Earlier studies have shown individual effect of exosomes and electrical stimulation in repair and regeneration of nerves [24,57–59]. Exosomes provides the necessary bioactive cues essential for nerve regeneration, whereas electrical stimulation is widely used as an adjunct therapy to enhance the therapeutic potential. BMSCs exosomes contain miRNAs and proteins which improves the functional recovery of the nerves by enhancing nerve remyelination, nerve fiber density, and nerve conduction velocity. In our study, we observed that after 6 weeks and 8 weeks, the Fused-Exo + ES group maintained the restored MNCV alike healthy control. After 6 weeks, the MNCV in the Fused-Exo + ES group was 56.76 ± 0.46 m/s, significantly higher than only Fused-Exo (49.03 ± 2.18 m/s) and Exo group (48.60 ± 1.18 m/s). Further, at the end of 8 weeks, there was a further improvement in the MNCV value of the Fused-Exo + ES (57.6 ± 0.45 m/s) compared to Exo (49.60 ± 0.95 m/s) group. These results demonstrated the therapeutic potential of fused exosomal therapy in improving the nerve conduction velocity, which was further enhanced by electrical stimulation and thus contributed to nerve regeneration. We also observed some improvement in MNCV in

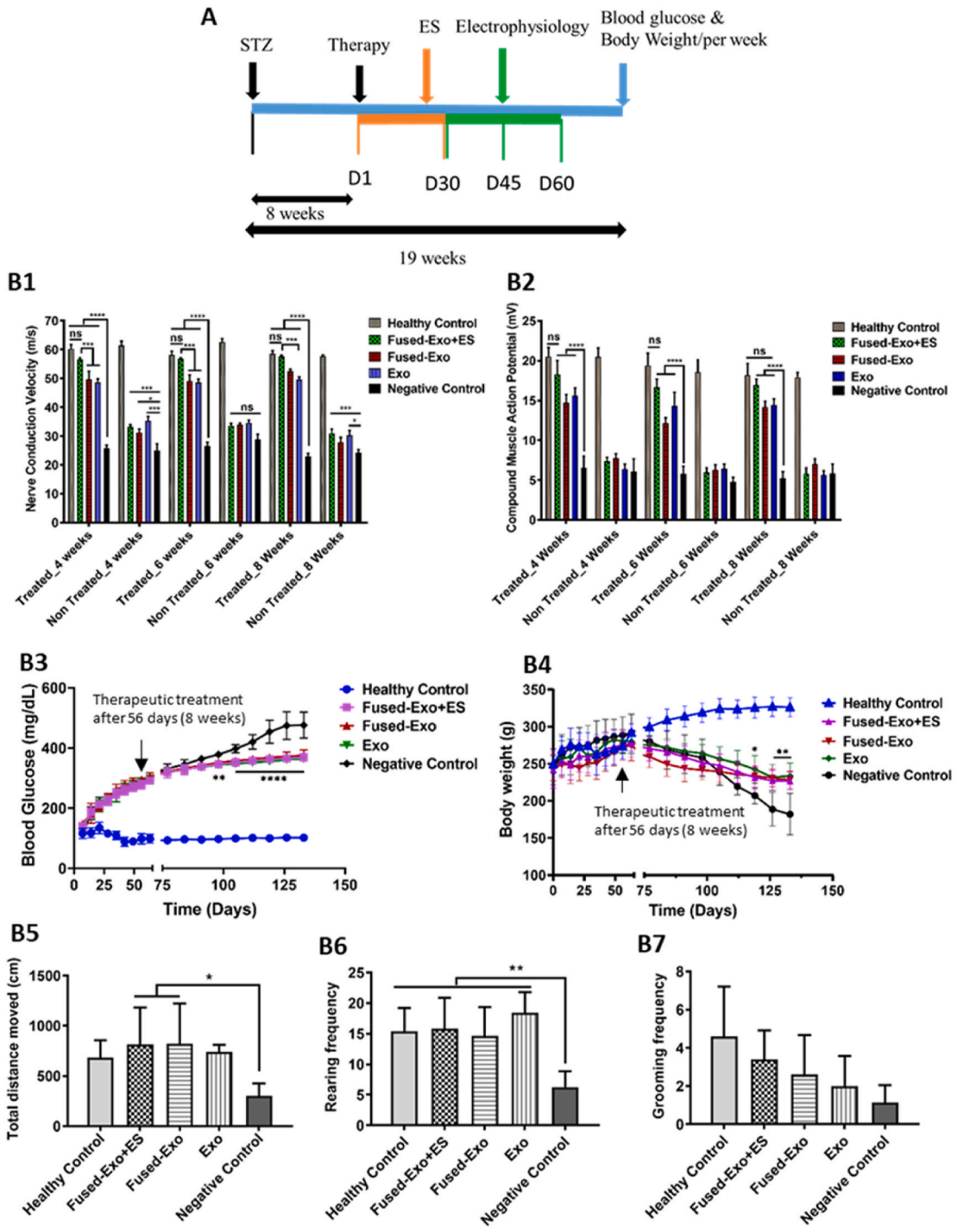

Fig. 5. The conducting exosomal therapy showed functional recovery, stabilized the blood glucose and body weight. (A) Scheme of the experimental protocol. Electrophysiological parameters (B1) nerve conduction velocity, and (B2) compound muscle action potential were measured after 4, 6, and 8 weeks after treatment of the treated (right) and non-treated (left) limb (B3) Blood glucose, and (B4) Bodyweight were measured every week throughout the experimental period. Behavioral analysis was done in the open field test by the measurement of (B5) total distance moved, (B6) rearing frequency, and (B7) grooming frequency for all the experimental groups after 8 weeks of treatment. *$p \leq 0.05$, **$p \leq 0.01$, ***$p \leq 0.001$ ****$p \leq 0.0001$.

the contralateral left limb of the treated animals, but they were not maintained with time. We next measured the amplitude of CMAP for all the experimental groups, which demonstrates the electrical activity of the muscle tissue. The amplitude values in all the three treated groups were found higher compared to the negative control group and un-treated contralateral left leg. After 4 weeks, the CMAP measured for the Fused-Exo + ES group (18.29 ± 1.74 mV) was significantly higher than the negative control group (6.57 ± 1.42 mV) (**Fig. 5 (B2)**). Also, the obtained CMAP in Fused-Exo + ES group was significantly increased than the Fused-Exo (14.68 ± 1.08 mV) and Exo group (15.62 ± 0.95 mV).

The increased amplitude in the Fused-Exo + ES group shows the combined role of fused exosomal therapy and ES in enhancing the regeneration of peripheral nerves. Application of ES is known to enhance amplitude and muscle action potential area after sciatic nerve injury in diabetic animals [24]. A similar trend was observed at the end

of 6 weeks, where the CMAP value of the Fused-Exo + ES (16.65 ± 1.02 mV) group was significantly higher than the Fused-Exo (12.16 ± 0.65 mV) group. However, after 8 weeks, the CMAP values of the healthy group (18.19 ± 1.45 mV), Fused-Exo + ES (16.96 ± 0.73 mV), Fused-Exo (14.19 ± 0.69 mV) and Exo (14.41 ± 0.80 mV) group were observed to be similar. The electrophysiological recordings of all the experimental groups after 8 weeks of exosomal therapy are represented in Fig. S4 (A). Taken together, the electrophysiology results revealed that the designer exosomes significantly improved the electrophysiological parameters of MNCV and CMAP in comparison to non-stimulated groups, which was further enhanced by electrical stimulation. The DCES, along with electrical stimulation, showed rapid functional recovery of damaged nerves indicating the synergistic effect of both exosomes and ES in enhancing nerve regeneration after DPN. For efficient disease manifestation of DPN, it is also essential to mitigate this condition as early as possible to avoid further complications. We observed enhanced and early improvement with the application of electrical stimulation along with fused exosomal therapy. Earlier, BMSCs transplanted in a diabetic neuropathy mice model enhanced the NCV after the treatment, however, the improvement lasted less than 4 weeks [60]. Also, intravenous injection of BMSCs derived exosomes for consecutive 8 weeks increased motor and sensory conduction velocities in DPN mice model [61]. However, the improvement was not comparable to that of non-diabetic mice. In comparison, our fused exosomal therapy was able to maintain nerve functional parameters over 8 weeks similar to healthy control, which is otherwise challenging. BMSCs derived exosomes have depicted that miRNA or combination of miRNAs and proteins present in them possesses neuroprotective response and play a vital role in gene regulation and biochemical signal transport [15,62,63]. BMSCs derived exosomes contain different miRNA's including miRNA-133b, and miRNA-17-92-cluster in the cargo that have shown enhanced nerve repair and regeneration [64,65]. These exosomal miRNA's enhance the nerve growth and functional recovery by activating different signalling pathways, such as activation of PTEN/mTOR signalling pathway, P13K/protein kinase B, and mediating RhoA and ERK1/2/CREB signal pathway [66]. These earlier studies have depicted role of MSCs derived exosomes in the nerve repair and regeneration, and it is likely that the observed effect in this study is partly due to these exosomal miRNA content being transferred to the cells [66].

Electrical stimulation (ES) of the nerve tissue has been used in clinics for the treatment of different neurological problems, including DPN. The ES is known to enhance the expression of neurotrophic factors and remyelination after nerve injury to support nerve repair and regeneration [59,67]. The actual mechanism behind how ES promotes improvement is still unclear. Different studies have evaluated the effect of ES in ameliorating DPN, however, the results have been inconsistent. Few studies demonstrated the role of ES in the improvement of NCV, while others indicated control in neuropathic pain only with no effect on electrophysiological parameters [68,69]. In the present study we have shown that ES along with DCES showed enhanced sciatic nerve functional improvements like NCV and CMAP than DCES and exosomes only. Polypyrrole has been predominantly used as an electrically conductive polymer in neural tissue regeneration [70]. The addition of conducting PpyNps and exogenous ES enhanced the electrical properties in the in-vivo system. Our results showed the role of ES in combination with conducting material in enhancing nerve regeneration. Designer exosomes-based therapy also offers a targeted delivery approach of the regenerative molecules to the specific injury sites. Targeting to the injury sites can be achieved by the expression of tissue specific target moieties on the exosomes [71]. For example, in case of nerve tissue, designer exosomes developed with neuron specific target peptide such as rabies viral glycoprotein (RVG) demonstrated enhanced targeted delivery of the cargo molecules to the neuronal cells when administered systemically [72]. Thus, conducting materials along with exosomes can be targeted better to the nerve injury sites by having targeted moieties on the exosomal system. We understand that the synergistic effect of exosomes, conducting PpyNps, and electrical stimulation lead to improved electrophysiological parameters after DPN. The therapeutic potential of DCES was further augmented when delivered in combination with exogeneous electrical stimulation improving the nerve conduction velocity, compound muscle actional potential, thus contributing to nerve regeneration.

2.5. Fused conducting exosomal system ameliorated hyperglycemia

Streptozotocin (STZ) is widely reported for the development of the T2DM animal model. The chemical structure of STZ comprises of a highly reactive nitrosourea moiety along with a glucose molecule that showed cytotoxicity. Glucose-mediated binding of nitrosourea to membrane receptor present on the β-cells commits structural damage. The glucose levels increased in all the groups after the induction of diabetes. Eight weeks after STZ administration, the diabetic rats showed significant hyperglycemia with a glucose level of 187.40 ± 20.54 mg/dL (Fused-Exo + ES), 182.90 ± 32.67 mg/dL (Fused-Exo), 185.80 ± 21.61 mg/dL (Exo) and 181.90 ± 20.48 mg/dL (negative control) as compared to 118.10 ± 16.26 mg/dL in healthy control group **(Fig. 5 (B3))**. After 5 weeks of a given therapy, a significant difference in glucose levels was observed between all the three treated groups, Fused-Exo + ES (338.20 ± 12.83 mg/dL), Fused-Exo (341.60 ± 11.98 mg/dL), and Exo (336.30 ± 12.37 mg/dL) as compared to the negative control group (363.90 ± 12.49 mg/dL). Interestingly, these differences were maintained throughout the study period after exosomal therapy. The results of the present study also represent damage to the pancreatic β-cells, thereby causing an increase in blood glucose level in STZ induced diabetic rats compared to healthy rats. Intriguingly, after giving an injection of DCES in diabetic animals induced with STZ, we observed that glucose level in all animals except negative control was maintained at a certain level with no significant further upsurge. However, it was higher as compared to healthy control animals. Exosomes could alleviate hyperglycemia by protecting pancreatic β-cells from apoptosis and promoting insulin sensitivity [23]. BMSCs derived exosomes are rich in enzymes needed for ATP synthesis of glycolysis such as glyceraldehydes 3-phosphate dehydrogenase (GAPDH), phosphoglucomutase (PGM), phosphoglycerate kinase (PGK), enolase along with a gene that encodes for 6-phosphofructo-2-kinase/fructose-2,6-biphosphatase [73]. The presence of these glycolytic enzymes may contribute to glycemic control in DCES and exosome treated animals. Although the local injection of the DCES was given intramuscularly, these exosomes might have traversed into the bloodstream, thereby contributed to glycemic control.

In the present study, diabetic rats exhibited a reduced body weight gain post-STZ injection compared to healthy animals **(Fig. 5 (B4))**. The reduction in body weight gain of STZ induced diabetic animals is due to the inability to metabolize the carbohydrate fuel sources and the wasting of the fat stores [74,75]. It was observed that after 4 weeks of therapeutic treatment, there was a decrease in body weight in animals with DPN as compared to the healthy groups. However, in the exosomal therapy treated animals, the weight loss was relatively less than the DPN control. After 9 weeks of the given treatment, there was a significant difference between the treated groups such as Fused-Exo + ES (231.50 ± 15.47 g), Fused-Exo (233.67 ± 11.10 g), and Exo (242.50 ± 18.33 g) as compared to the negative control group (207.00 ± 11.17 g) in the body weight. These differences were maintained until the end of the study, indicating the role of the given exosomal therapy in controlling instant loss in body weight and correlated with the hyperglycemic control. These observations indicated the long-term therapeutic effects of exosomal treatment.

2.6. Behavioral analysis: open field test

The effect of DCES on the DPN animal model in the open field test is represented in Fig. 5 (B5–B7). Interestingly, post-therapy, we found that the animals in the Fused-Exo + ES, Fused-Exo, and Exo group were more

active and traveled more distance in the open field test compared to the negative control group **(Fig. 5 (B5))**. The negative control group showed the least distance moved due to damage to nerves affecting the sensory and motor functions. Rearing frequency (RF) is the frequency with which rats stand using the hind legs and indicates the locomotor activity. The frequency of rearing in all the treated groups was similar to the healthy control group and significantly high as compared to the negative control **(Fig. 5 (B6))**. It was demonstrated that exosomal therapy had maintained the locomotor activity near the normal and lower level of anxiety after DPN. Further, grooming is a behavior of rodents evident by body care, self-calming activities, displacement, and comforts. No significant difference in grooming frequency (GF) between the experimental groups was seen **(Fig. 5 (B7))**. All these activities are coordinated by the nervous system; however, in a diseased state of DPN, loss, and damage to nerves contribute to reduced RF and GF. DCES therapy proves beneficial in restoring the normal behavior function of animals. Taken together, these results of behavioral analysis, it was concluded that designer exosomal therapy improves the behavior and nerve function after DPN.

2.7. Histological and immunostaining analysis for peripheral nerve regeneration

To examine the histological changes in the peripheral sciatic nerve, toluidine blue staining of the middle segment of the sciatic nerve was performed (Fig. 6A). The morphology and structure of sciatic nerve fibers in all three treated groups, Fused-Exo + ES, Fused-Exo, and Exo was found similar with partial restoration of nerve fiber morphology. This restoration is due to the neuroprotective effect of delivered exosomal therapy and ES which enhances the proliferation of Schwann cells,

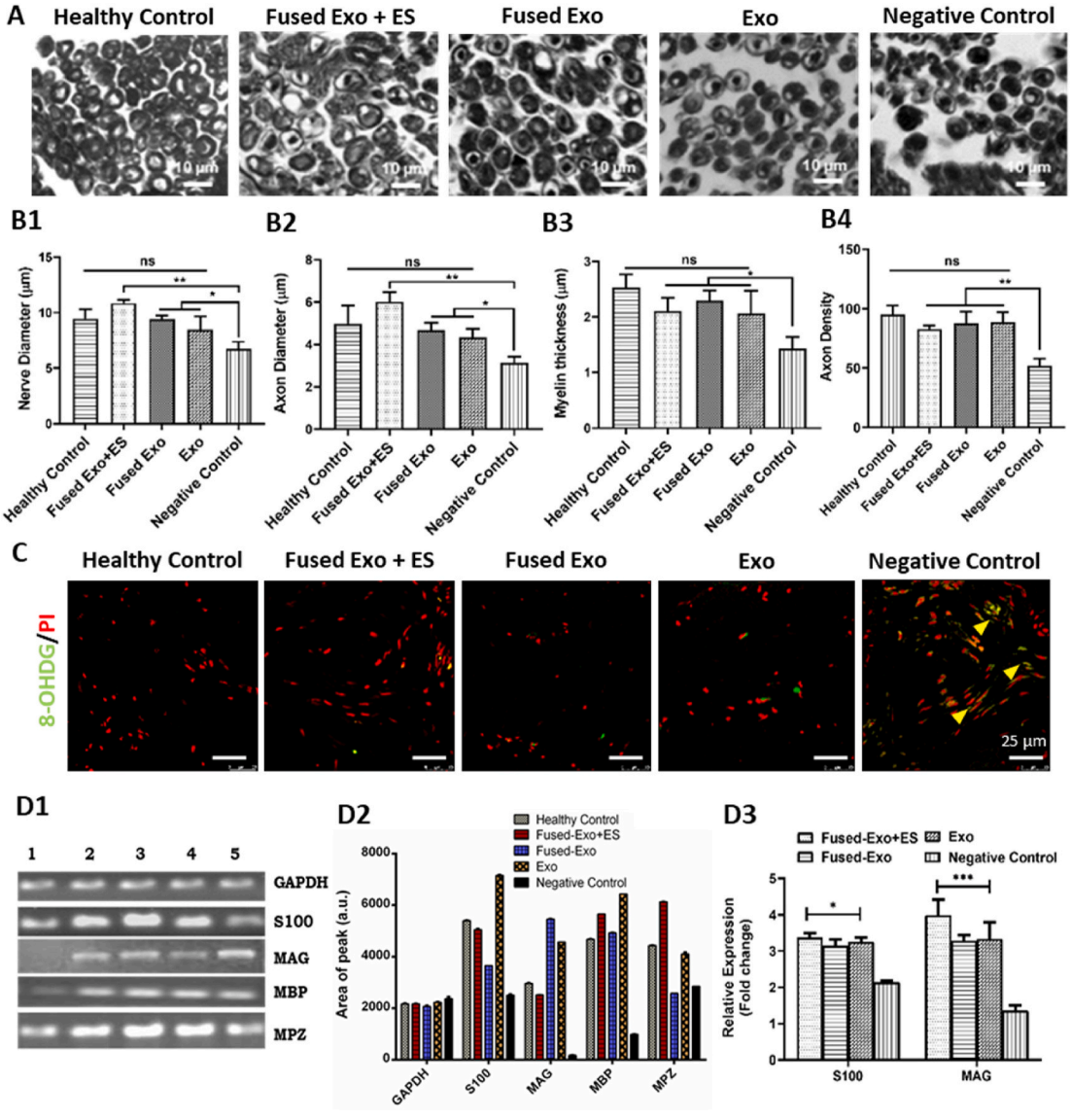

Fig. 6. (A) Histopathology (Toluidine blue staining) of isolated sciatic nerve samples showing improvement in the tissue organization and anatomy in the treated groups compared to the negative control group after 8 weeks of exosomal therapy at 100x magnification. Nerve morphometric analysis of the toluidine blue-stained images from all the experimental groups for (B1) nerve diameter, (B2) axon diameter, (B3) myelin thickness, and (B4) axon density. (C) Sciatic nerve transverse sections from the different experimental groups were observed in immunofluorescence-stained images against the 8-OHDG oxidative stress marker at 40x magnification. The yellow arrows indicate 8-OHDG expression (green) in the negative control group. Gene expression analysis in sciatic nerve samples after 8 weeks of therapy (D1) Semi-quantitative gene expression analysis of the sciatic nerve samples in, (1) Negative control, (2) Healthy control, (3) Exo, (4) Fused-Exo + ES, (5) Fused-Exo, (D2) quantification of the gene expression based on the semi-quantitative expression analysis. (D3) Graph representing relative gene expression based on the qRT-PCR analysis. *$p \leq 0.05$, **$p \leq 0.01$, ***$p \leq 0.001$, ns: non-significant.

remyelination, and axonal regeneration [76]. We observed significant improvement in nerve diameter, axon diameter, myelin thickness, and axon density in the treated groups as compared to the negative control group **(Fig. 6 (B1–B4))**. Further, sustained glycemic control due to exosomal delivery improved the nerve morphology affected due to DPN. In the negative control, there was a prominent decrease in the axon density along with expanded lamellar spaces as compared to treated groups ($p \leq 0.01$). The sciatic nerve fibers with expanded lamellar spaces reflected the visible sign of axonal atrophy. After exosomal therapy, prominent regenerative changes were observed due to the uptake of cargo by neuronal cells, which produced the immediate effect. Possession of neuroprotective cues in BMSCs derived exosomes contribute to this restoration of nerve morphology [13].

Hyperglycemia leads to altered protein structure of the mitochondrial electron transport chain leading to the development of oxidative stress by the generation of ROS and peroxides [77,78]. It also suppresses the mitochondrial antioxidants such as superoxide dismutase and glutathione peroxidase. Therefore, we analyzed the presence of oxidative stress in the sciatic nerve after DPN. 8-OHDG (8-hydroxy-2′-deoxyguanosine) is one such DNA oxidative stress marker, which indicates the extent of oxidative damage in the nerve.

We did immunostaining for the 8-OHDG marker and the immunofluorescence images showed less expression in all the groups receiving exosomal therapy than the negative control group **(Fig. 6C)**. Similar results were obtained in the quantitative analysis showing significantly more expression of the 8-OHDG stress marker in the DPN control than the treated groups (Fig. S4 (B)). This indicates that the oxidative stress generated after DPN has been controlled by our exosomal therapy, whereas the stress is maintained in the untreated negative control group. Exosomes transfer heat shock proteins (protective proteins), glycolytic enzymes, genetic information in the form of RNA, proteins deciphering antioxidant activities to reduce oxidative stress [79,80]. BMSCs derived exosomes have antioxidants such as glutathione-S-transferases and peroxiredoxins to supplement the cellular antioxidants [81]. The exosomal treatment has reduced the oxidative stress in the treated groups because of their antioxidant activity.

2.8. Gene expression analysis

The generation of DPN leads to nerve damage which is mostly associated with altered expression of myelin-specific proteins like MAG, MBP, and MPZ, along with Schwann cells associated S100 protein [82]. Therefore, we analyzed whether there was any effect of exosomal therapy on the expression of SCs and myelin-specific proteins. Expression of S100, myelin-associated glycoprotein (MAG), myelin basic protein (MBP), myelin protein zero (MPZ), and GAPDH genes, were analyzed in all the groups by semi-quantitative gene expression analysis. There was an increased gene expression of S100, MAG, MBP, and MPZ after exosomal therapy compared to the negative control **(Fig. 6 (D1-D2))**. These observations indicate the role of exosomal therapy in enhancing remyelination. We further analyzed the gene expression of the Schwann cell marker, S100, and myelin-associated glycoprotein, MAG by quantitative real-time RT-PCR (qRT-PCR). The given therapy significantly upregulated S100 gene expression in the treated groups as compared to the negative control ($p \leq 0.05$). Increased S100 expression indicates the proliferation of the Schwann cells after the exosomal therapy. SCs play an essential role in nerve regeneration by secreting growth factors, supporting remyelination and axonal regeneration after injury [83]. SCs secrete myelin proteins such as MAG, which is important to develop and maintain myelin in the nerve tissue [84]. DPN causes damage to the SCs resulting in demyelination and down regulation of myelin proteins. Also decrease in the nerve conduction velocity indicates the damage in the myelin sheath in sciatic nerve after diabetic neuropathy. We observed down regulation of MAG in the sciatic nerve after DPN in the non-treated negative control **(Fig. 6 (D3))**. However, a significant increase in MAG was observed in the sciatic nerve after exosomal therapy in comparison to the negative control ($p \leq 0.001$) **(Fig. 6 (D3))**. The increased expression of these markers indicates that the given exosomal therapy has modulated SCs and myelination related gene expression. This increased expression in Schwann cell and myelin-associated proteins, which corresponds to the remyelination and axonal regeneration, corroborates to the improvement in nerve functionality (NCV) and nerve morphology as observed in earlier electrophysiology results.

2.9. Fused conducting exosomal system augmented muscle regeneration

The gastrocnemius muscle (GM) is the class of skeletal muscle, which is innervated by the sciatic nerve, and it degenerates after diabetic neuropathy. Sciatic nerve regeneration and reinnervation of the GM, attenuates the muscle atrophy. We assessed the muscle atrophy and regeneration by GM weight analysis, and Masson's trichrome staining which indicates about the extracellular matrix (ECM) deposition in the tissue. Exosomal therapy restored muscle morphology, muscle mass, and integrity. The treated groups showed integrated muscle fiber morphology similar to the healthy control group. In the negative control group, extensive collagen deposition (blue color), reduced muscle mass, and disintegrated muscle matrix due to a reduction in muscle fiber size was observed compared to the treated group (Fig. 7A). Hyperglycemia induced oxidative stress is one of the main players associated with muscle atrophy. Earlier studies have shown that attenuation of oxidative stress using antioxidant biomolecules have prevented muscle atrophy in DPN [85,86]. Exosomes as demonstrated in our in-vitro studies attenuated oxidative stress, which may have prevented GM atrophy. Further, in earlier clinical and pre-clinical studies, electrical stimulation has prevented diabetes associated muscle atrophy in diabetic patients as well as preclinical animal studies [87,88]. Therefore, exosomes along with electrical stimulation may be a more effective treatment in mitigating DPN along with muscle atrophy. However further mechanistic understanding is required to reveal its true potential. We also studied the effect of exosomal therapy in inducing the cellular proliferation of the injured GM. Proliferating cell nuclear antigen (PCNA), a marker for cellular proliferation, was analyzed in both the transverse and longitudinal GM sections after neuropathy **(Fig. 7 (B1))**. We observed that treated groups showed high cellular proliferation activity compared to the negative control group in both the transverse **(Fig. 7 (B2))** and longitudinal sections **(Fig. 7 (B3))**. After muscle injury, satellite cells, which are the stem cells, divide and differentiate to restore and regenerate the lost muscle fibers [89]. Because of the hyperglycemic condition, these satellite cells display reduced proliferative and regenerative capability in the damaged muscle tissue. It has recently been shown that exosomes enhanced the activation, proliferation, and differentiation of the satellite cells by ERK phosphorylation [90]. The exosomal therapy might have activated these satellite cells and enhanced their division and differentiation into muscle cells, leading to muscle regeneration. The digital images of the isolated gastrocnemius muscles from all the experimental groups are represented in Fig. 7 (C1). We observed that our exosomal therapy has attenuated the muscle atrophy and, recovered and regenerated the muscle tissue after DPN. Conversely, we observed severe muscle degeneration in the negative control group. This was further supported by quantifying the GM weight ratio. As indicated in the quantification data **(Fig. 7 (C2))**, there was a significant difference in the GM weight of the treated groups; Fused-Exo + ES (1.430 ± 0.136 g), Fused-Exo (1.351 ± 0.197 g), and Exo (1.432 ± 0.144 g), as compared to the untreated negative control group (0.704 ± 0.179 g). Collectively, these results indicated the effect of fused exosomal therapy and electrical stimulation in ameliorating DPN, enhancing nerve regeneration and recovering muscle tissue atrophy.

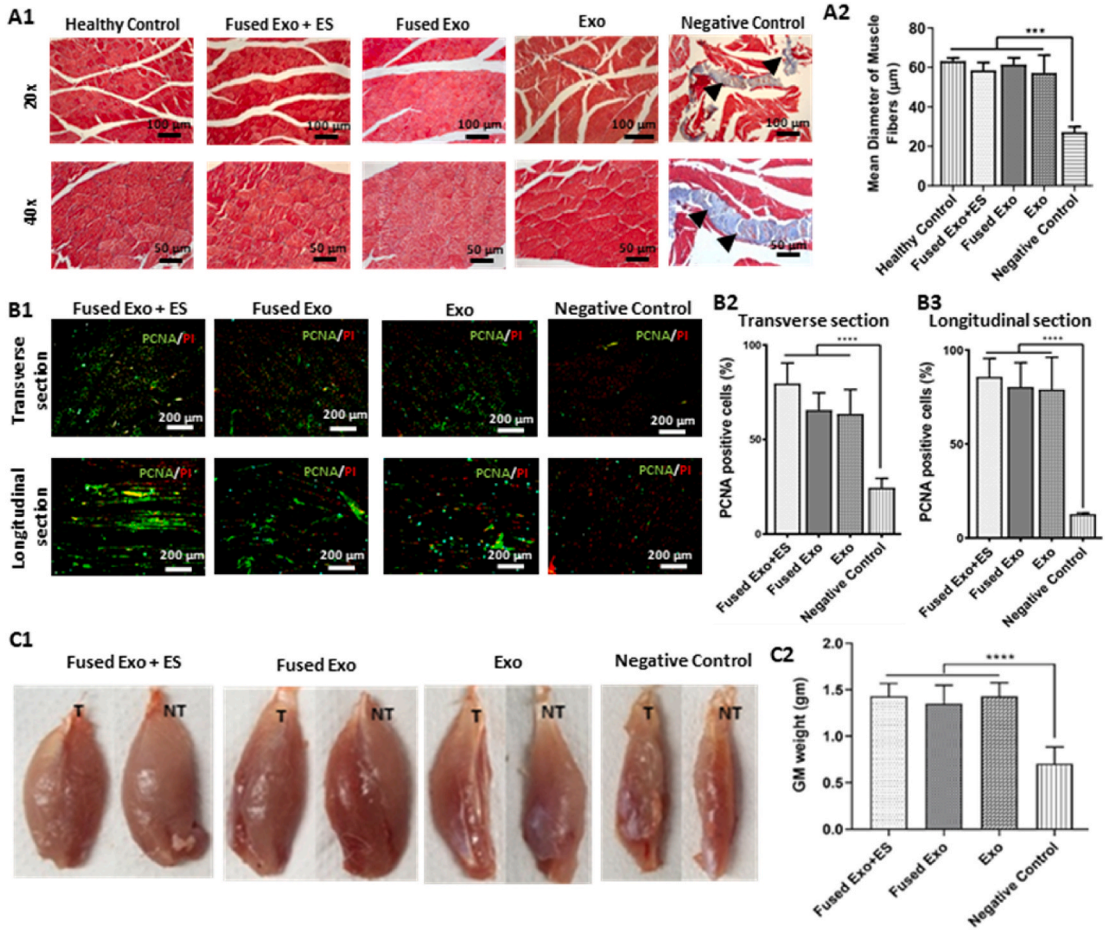

Fig. 7. Exosomal therapy promoted gastrocnemius muscle regeneration after DPN. (A1) Masson's trichrome stained images of the gastrocnemius muscle of the treated limb (right) after 8 weeks of therapy at 20x and 40x magnification, (A2) Quantification of the mean diameter of the muscle fibers. PCNA marker expression in the transverse and longitudinal gastrocnemius muscle sections from the different experimental groups, (B1) confocal immunofluorescence images representing PCNA marker expression. Quantification of the PCNA marker expression in (B2) transverse sections, and (B3) longitudinal sections. (C1) Representative images of the isolated gastrocnemius muscles from different experimental groups, T (treated) and NT (Non-treated), and (C2) quantification of the muscle weight from the treated hind limb (right). ****$p \leq 0.0001$.

2.10. Fused conducting exosomal system enhanced the recovery of pancreas, kidney, and liver after diabetic peripheral neuropathy

After STZ administration, hyperglycemia causes severe cellular destruction in the pancreas, kidney, and liver tissues [91]. In pancreatic tissue, the untreated negative control group showed a decrease in pancreatic cell mass, disrupted tissue architecture, and severe inflammation compared to the healthy pancreatic tissue (Fig. 8). After the exosomal therapy, improvements in the pancreatic tissues were observed in the Exo, Fused-Exo, and Fused-Exo + ES group, which was evident by the maintenance of the integrity, and the presence of islets of Langerhans. The exosomal therapy also enhanced pancreatic cell proliferation after DPN as observed in PCNA immunostaining (Fig. S5). The treated groups showed significant cellular proliferation as compared to the non-treated group. Exosomes derived from mesenchymal stem cells are known to have the potential to enhance cellular proliferation after tissue injury [92]. BMSCs derived exosomes might have protected the pancreatic tissue against degeneration by inducing β-cell proliferation and inhibiting cellular apoptosis. The changes in kidney cortex histology are shown in the H&E-stained images (Fig. 8). The healthy control group showed the typical kidney architecture, glomerular augmentation, and matrix arrangement compared to negative control animals that have deformed renal tubular epithelial cells, vacuolated degeneration and necrosis, and glycogen deposition. However, after treatment, tissue recovery was observed with normal glomeruli structure similar to healthy control. The exosomal therapy also enhanced the renal tissue recovery by promoting cellular proliferation as observed in PCNA immunostaining results of the kidney sections (Fig. S6). Stem cell-derived exosomes have the potential to repress cellular apoptosis and promote renal cell proliferation [93,94]. After the administration of STZ, degenerative changes such as vacuolated spaces, inflammation, and hemorrhage were observed in the hepatic cells in liver tissue of the negative control group. However, in the treated groups, exosomal therapy partially recovered the liver tissue with some inflammation in the Exo group **(Fig. 8)**. These results indicate a systemic protective effect of exosomal therapy in various peripheral organs, which needs to be studied further.

In summary, we have successfully developed designer conducting exosomal system (DCES) and demonstrated a combined effect of fused exosomes and electrical stimulation in ameliorating diabetic peripheral neuropathy (DPN). In electrophysiological studies, exosomes significantly enhanced the electrophysiological parameters such as NCV and CMAP, which were significantly better than the negative control. However, fused exosomes in the form of DCES along with electrical stimulation further improved these electrophysiological parameters. The results demonstrated a significant effect of both exosomes and electrical stimulation in nerve regeneration at electrophysiological level. Interestingly, at the cellular/molecular level, we again observed a prominent effect of exosomes on histopathology, but could not be enhanced by additional electrical stimulation. Similar trend was also observed in gene expression analysis, where exosomes promoted the

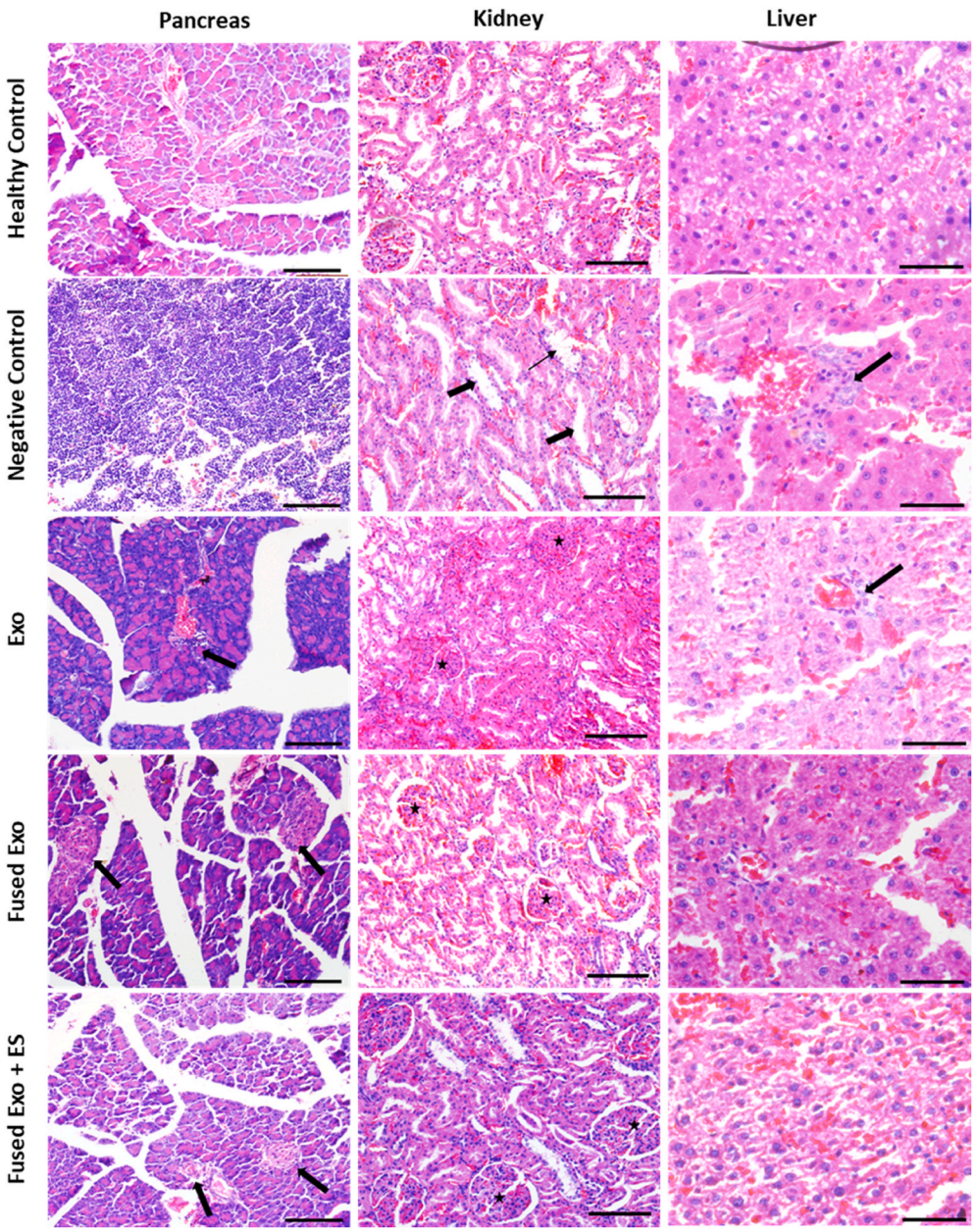

Fig. 8. Histological and morphological analysis of the different tissues by H&E staining after 8 weeks of therapy. In the pancreas, normal tissue morphology was observed in the healthy control, whereas distorted tissue architecture with severe inflammation and necrosis was observed in the negative control. In Exo, Fused-Exo, and Fused-Exo + ES group, islets of Langerhans (black arrows) were observed with partial tissue recovery, scale bar: 100 μm. In the case of the kidney, normal tissue architecture was observed for healthy control, whereas vacuolar degeneration and necrosis in renal tubular cells (thick arrows), and glycogen deposition (thin arrows) were observed in the negative control. In Exo, Fused-Exo, and Fused-Exo + ES group, normal glomeruli were observed (stars) similar to healthy control, scale bar: 100 μm. In liver tissue, normal liver morphology was observed in the healthy control, whereas severe inflammation (black arrows) was observed in the negative control. Some inflammation was observed in the Exo group (black arrow), with partial tissue recovery in the Fused-Exo and Fused-Exo + ES group, scale bar: 50 μm.

expression of S100 and MAG genes, but no further increased expression was observed after electrical stimulation. These results demonstrated that exosomes have prominent effect at cellular/molecular level by modulating the gene expression and histopathology, while electrical stimulation has more role to play in modulation of electrophysiological parameters. Our results are the first step in the development of a combinatorial therapeutic approach that can be translated to clinics. To further establish this concept and to understand the overall potential of the therapy, many future questions remain to be addressed. The mechanistic understanding and role of exosomes and electrical stimulation in treating DPN needs to be elucidated. Although electrical stimulation enhanced the effect of fused exosomes, the individual benefits of electrical stimulation with and without conducting nanoparticles and exosomes needs to be elucidated. Further taking lead from these results, a detailed investigation into the systemic effect of the developed therapy is also being carried out.

3. Conclusion

Diabetic peripheral neuropathy leads to severe nerve damage and can't be recovered to a healthy state without effective therapy. Our results demonstrated that the developed designer conducting exosomal treatment and the short duration of ES enhanced recovery of the damaged nerves affected with diabetic peripheral neuropathy (DPN). Delivering BMSCs derived exosomes and conducting system such as polypyrrole nanoparticles and exogenous electrical stimulation have been proving a new emerging treatment approach in therapeutic and regenerative therapy. The DCES interplays in the reversal of nerve tissue damage and DPN manifestations and also a proven anti-hyperglycemic role. Our results also suggest an exosomal role in glycemic control, which needs further investigation. Moreover, further clinical trials are necessary to optimize their use in clinics.

4. Experimental section

4.1. Materials

All chemicals and reagents used were purchased from Merck, USA, or otherwise mentioned and detailed in supporting information.

4.2. Exosomes isolation and characterization

Exosomes were isolated from bone marrow mesenchymal stromal cells (BMSCs) using differential centrifugation and micro-filtration [42]. BMSCs were isolated from Wistar rats as described in supporting information. Once the BMSCs in passage 4 reached 70–80% confluency, complete medium was replaced with serum-free medium supplemented with 1% antibiotic, and cells were cultured for 48 h. After 48 h, the spent media was collected to isolate exosomes. The spent media was centrifuged at 2000 x g for 10 min to remove the cell debris. The supernatant was collected and centrifuged at 16,000 x g for 40 min to remove the microvesicles. The collected supernatant was concentrated using Amicon® Ultra Centrifugal filters (100 kDa MWCO) at 2000g, and the final protein concentration was determined using BCA protein assay (Pierce, ThermoScientific, USA). Confocal microscopy, field emission scanning electron microscopy (FESEM) and transmission electron microscopy (TEM) and cryo-TEM were used to visualize the exosomes. Nanotracking analysis (NTA) was performed to determine the size distribution and concentration of exosomes with 488 laser. Triplicate measurements of each sample (30 s) were recorded with a camera level of 14 and a detection threshold of at 10. For analyzing the exosomal surface markers, Western blot analysis for CD81, CD9, and β-actin was done as described in supporting information. Exosomes were also analyzed by immunogold labeling and analyzed by TEM as per the details in supporting information.

4.3. Synthesis of liposomes and packaging of PpyNps

Polypyrrole nanoparticles (PpyNps) were synthesized by the chemical oxidation polymerization reaction, as reported elsewhere [36] and detailed in supporting information. Liposomes were synthesized using the film hydration method, as reported elsewhere [36]. Briefly, the lipids including DPPC, cholesterol, CHEMS (70:5:17.25 M ratio) were dissolved in dichloromethane and methanol (5 mL, 4:1 v/v). The round bottom flask containing the lipid components was placed under a rotary evaporator (BUCHI™ Rotavapor™ R-210 Rotary Evaporator System, Fischer Scientific, Thermo Scientific, USA). After removing the solvent, a thin lipid film at the surface formed was hydrated with a 5% w/v dextrose solution containing PpyNps at ratio 1:2 (w/w lipid: PpyNps), followed by ultraprobe sonication for 2 h in ice. Furthermore, the packaged liposomes loaded with PpyNps were passed through a 0.22 μm (Millipore) syringe filter to remove the microparticle size components, followed by the removal of free PpyNps with Sephadex G-25 column (Sigma-Aldrich, St. Louis, MO, USA). The incorporation of PpyNps was confirmed by UV spectroscopy within the wavelength range of 400–800 nm. Confocal microscopy (LSM780NLO, Carl Zeiss GmbH, Germany), and FESEM was used to visualize the liposomes described earlier. These particles are designated as polypyrrole nanoparticles containing liposomes. Exosomes were also analyzed through liquid chromatography-mass spectroscopic (LC-MS/MS) analysis as per the methodology reported in supporting information.

4.4. Exosome labeling with PKH-26 and Calcein-AM dyes

The isolated BMSCs exosomes were labeled with PKH-26 (Red Fluorescent Cell Linker, Sigma Aldrich) as per the manufacturer's protocol. Briefly, the isolated EVs were incubated with 3 μM of fluorescent PKH-26 dye in dilution buffer at room temperature, followed by density gradient ultracentrifugation at 192000 g for 2 h at 4 °C. The supernatant was carefully removed, and the labeled exosomes pellet was resuspended in the 1X PBS buffer or culture media as per requirement. To detect the intact exosomes vesicles, Calcein-AM staining was performed. The EVs were labeled with Calcein-AM (10 μM) working concentration in PBS and incubated at 37 °C for 20 min. The unlabeled dye was removed by centrifuging in 100 KDa filters (Amicon). The cells were incubated with Calcein-AM labeled exosomes at 37 °C. Further, the cells were washed with 1X PBS (3X), and the images were taken using a confocal microscope (Leica SPII, Germany).

4.5. Fusion of exosomes and packaged PpyNps containing liposomes

The exosome and liposome membranes were fused using the freeze-thaw method [42]. For effective fusion, the exosomes were mixed with liposomes in the ratio 2:1 (number of exosomes to the number of liposomes). The mixtures were frozen in liquid nitrogen and thawed at 50 °C in a water bath for 15 min/cycle. The freeze-thaw process was repeated ten times. TEM (FEI Technai G2 12 Twin TEM 120 kV) analysis was performed to visualize the exosomes fusion with liposomes. The fused exosomes and liposomes were loaded on the holey carbon grid and visualized for the immunogold labeling against the CD-9 marker in TEM. The membrane fusion was also viewed with confocal microscopy. Briefly, exosomes labeled with PKH26 (Red Fluorescent Cell Linker, Sigma Aldrich) were fused with liposomes labeled with PKH67 (Green Fluorescent Cell Linker, Sigma Aldrich) for visualization under a fluorescence microscope. The fusion efficiency between the liposomes and exosomes vesicles was measured using the R18 (Rhodamine B octadecyl ester perchlorate) (Sigma Aldrich) fusion assay. The R18 stock solution (1 mg/ml) was prepared in methanol. Briefly, 100 μl of liposomes (5×10^5) were labeled with a range of R18 (0.5–4 μl) at RT for 1 h under gentle shaking. The unlabeled dye was removed by ultracentrifugation at 190000 g at 4 °C for 2 h. The labeled liposomes were dissolved in 100 μl PBS and mixed with 100 μl of exosomes (1×10^6) in PBS. The exosomes and liposomes were fused together under freeze-thawing. The fluorescence of the fused vesicles was measured at an excitation of 554 nm and an emission of 575 nm. Finally, 20 μl Triton X-100 was added to measure the fluorescence at infinite dilution. The fusion efficiency between the two vesicles was determined using equation (1).

$$\text{Fusion efficiency} = (\text{Ft}) - (\text{F0})/(\text{F}) - (\text{F0}) \quad (1)$$

Where, Ft = Fluorescence after fusion, F0 = Fluorescence before fusion and F = Fluorescence at infinite dilution.

4.6. Exosomes internalization studies in SH-SY5Y cells and Neuro2a cells

The exosome internalization was studied in neuroblastoma cell lines, SH-SY5Y (NCCS Pune, India), and Neuro2a cell lines. SH-SY5Y are human neuroblastoma cells, cultured in Opti-MEM (Gibco, Thermo Fisher Scientific) supplemented with 5% FBS and 1% penicillin-streptomycin antibiotic solution, and Neuro2a cells were cultured in DMEM culture media supplemented with 10% FBS and 1% antibiotic solution. Both SH-SY5Y and Neuro2a cells were seeded in 35 mm confocal dishes (ibidi) at a density of 5×10^3 cells and incubated for 24 h at 37 °C. Further, the cells were co-cultured with the labeled exosomes and fused exosomes and incubated for 30 min at 37 °C. Finally, live-cell imaging was performed using a confocal microscope (Leica SPII, Germany) followed by staining of cells with the nuclear stain DAPI and Phalloidin-FITC for actin visualization. The fluorescence intensity of the internalized exosomes was calculated by using the confocal fluorescence images of the exosomes and fused exosomes internalized by the SH-SY5Y cells. Total fluorescence intensity of the internalized exosomes and fused exosomes was measured by analyzing 5–6 images in the ImageJ software.

4.7. Oxidative stress studies through high glucose toxicity and menadione treatment

For high glucose toxicity studies, SH-SY5Y cells were seeded in 96 well plate at a density of 5×10^3 cells/well. After 24 h of cell seeding, the cells were incubated with exosomes (30 μg/ml). Similarly, SH-SY5Y cells (2×10^4 cells/well) were seeded and incubated with fused exosomes (30 μg/ml). Further, after 24 h, the cells were treated with high glucose (150 mM) in Opti-MEM media. As a control, cells were cultured in high-glucose conditions without exosomes treatment. MTT assay was done at different time intervals to measure metabolic activity. A live/dead cell integrity assay was carried out using Calcein-AM/PI after 48 h and 72 h, and the images were quantified using ImageJ software. For oxidative stress study, Neuro2a cells were seeded at a density of 5×10^3 cells/well. After 24 h of cell seeding, the cells were incubated with exosomes (30 μg/ml). Further, after 24 h of exosome treatment, the cells were treated with menadione (20 μM) in DMEM media under serum-free conditions. For cellular viability, MTT assay was carried out every 2 h after 4 h of treatment consecutively till 12 h. Live/dead imaging was performed after 12 h using Calcein-AM/PI staining.

4.8. Induction of diabetic peripheral neuropathy and animal treatment

Female Wistar rats (n = 50), 12–14 weeks old, having bodyweight of 200–250 g were selected and acclimatized as per ethical guidelines. DPN was induced by intraperitoneal (IP) injection of STZ (65 mg/kg prepared in 100 mmol/L sodium citrate buffer, pH = 4.5) at three subsequent doses on alternate days. One-week post-STZ injection, weekly fasting blood glucose (FBG) was measured by glucometer (Glucocare™, Ultima, RMD Mediaids Limited, India) every week, ensuring the induction of diabetes. For glucose measurements, the rats were kept in a restrainer, and the prick tail snipping method was employed to check FBG (from a drop of blood) (FBG≥200 mg/dL). To confirm the development of DPN, electrophysiological parameters were measured after induction of diabetes at every 15th day using electromyogram (EMG) (Nicolet® EDX, Natus Medical Incorporated, Pleasanton, CA 94566 USA) [95]. Briefly, the animals were anesthetized using isoflurane gas (2–4%), and the hind limbs were shaved and cleaned. The sciatic nerve was stimulated using a recording electrode through proximal stimulation close to the sciatic notch and distal stimulations close to the knee using bipolar needle electrodes. The recording electrode was placed at the gastrocnemius muscle. A reference electrode was placed between the stimulating and recording electrode, and the ground electrode was placed at the tail. After confirming DPN, the animals were randomly assigned in equal numbers to four experimental groups (n = 10, each group) and a healthy control group. The five experimental groups were (1) Fused-Exo + ES, (2) Fused-Exo, (3) Exo, (4) Negative control, and (5) Healthy control, as mentioned in Table 1. After DPN, the group 1 (Fused-Exo + ES) and group 2 (Fused-Exo) animals were given an injection of 20 μg/ml of fused exosomes in 5% w/v dextrose solution into the right hind limb muscles with a sterilized syringe attached with the needle of 25-gauge at three points dispensing 167 μl volume at each point. In group 3 (Exo), exosomes (20 μg/ml), and in group 4 (Negative control), 5% dextrose was injected. In group 5 (Healthy control), the non-diabetic animals have also injected with 5% dextrose only. The left hind limb served as contralateral control and injected with 5% dextrose only in all the experimental groups. To keep exosome amount similar in all groups, we used an equal amount of exosomes to fuse with liposomes to develop the fused product for the therapy. Weekly fasting blood glucose (FBG) and body weight (BW) was recorded up to the termination of the experiment. Post-injection in group 1 (Fused-Exo + ES), electrical stimulation (ES) therapy (Nicolet® EDX, Natus Medical Incorporated, USA) was given subsequently on alternate days for one month. Briefly, the positive and negative electrodes were inserted near the hip joint and knee, respectively. The electrical stimulation was given to the animals at 2 Hz frequency and 1 mA current, producing visible muscle contraction for 15 min [96]. The electrophysiology parameters were measured every 15th-day post-treatment for eight weeks.

Table 1
Experimental groups used in the animal study.

S. No.	Animal Groups	Number of animals	Description of the given therapy	
			Right Limb	Left Limb
1.	Fused-Exo + ES	10	Exosomes fused with polypyrrole NPs containing liposomes along with exogenous electrical stimulation	Dextrose only
2.	Fused-Exo	10	Exosomes fused with polypyrrole NPs containing liposomes	Dextrose only
3.	Exo	10	Exosomes only	Dextrose only
4.	Negative Control	10	Dextrose only	Dextrose only
5.	Healthy Control	10	Dextrose only	Dextrose only

4.9. Behavioral studies- open field test

An open field test was performed to analyze the behavioral changes in the animals after DPN. The animals were examined for anxiety, locomotion, and exploring behavior. Horizontal and vertical activities of the rats were recorded for a time period of 5 min through a high-definition video recording camera. Then the video was analyzed for behavioral analysis [97]. Briefly, the animals were placed in a glass box area [56 × 56 × 20 cm], and its floor was divided into 16 small squares that permit the definition of central and peripheral parts. The animals were acclimatized to the apparatus before the actual recording. At the start of the procedure, each animal was placed in the center of the box, and its activity was recorded, and the following behavioral parameters were scored, (1) total distance moved (cm), (2) grooming frequency, and (3) rearing frequency. The procedure was repeated three times for each animal of all the experimental groups.

4.10. Animal sacrifice and histological analysis

Eleven weeks after treatment, animals were sacrificed using an overdose of pentobarbital (15 mg/100 g) followed by cervical dislocation. The sciatic nerve, gastrocnemius muscle, liver, kidney, and pancreas were collected and fixed in 10% formalin. The moist weight of the isolated gastrocnemius muscle from the treated hindlimb (right) was measured immediately after the animals were sacrificed. Histological analysis was carried out through H and E staining as detailed in the supporting information.

4.11. Immunofluorescence staining and gene expression analysis

Immunostaining was performed on the isolated sciatic nerve transverse sections (4–5 μm thickness) for 8-OHDG (1:200, Santa Cruz), as described in supporting information. The gastrocnemius muscle, kidney, liver, and pancreas sections were immunostained for PCNA (1:50, Santa Cruz) marker analysis. Gene expression analysis was carried out for S100, MAG, MBP, and MPZ with GAPDH as internal control as per the detailed methodology reported in supporting information.

4.12. Statistical analysis

All the in-vitro experiments were carried out in triplicates having a minimum sample size of n = 3. All the quantitative analysis was carried out using GraphPad Prism 8.0 using two-tailed student's t-test and ANOVA tests. For the multiple comparison test, One-way and Two-way ANOVA tests were used in GraphPad prism. Each experimental group

was compared to all other groups at each time point in case of electrophysiology data by Two-way ANOVA test. One-way ANOVA test was used for nerve morphometry and muscle analysis. The *p*-value of less than 0.05 was considered statistically significant.

4.13. Animal ethics statement

Animal experiments were performed as per guideline laid down by Committee for the Purpose of Control and Supervision of Experiments on Animals (CPCSEA), and Institutional Animal Ethics Committee (IAEC) using the approval numbers IITK/IAEC/2014/1025 and IITK/IAEC/2017/1064 of the Indian Institute of Technology Kanpur, India.

Author contributions

A.K., A.S., and A.R., designed and planned the whole study and experimental plan. A.S., A.R., and P.A.S., performed the experimental work and the analysis of the results. A.S. and A.R. wrote the manuscript, and A.K. reviewed it.

Data availability

The raw/processed data required to reproduce these findings cannot be shared at this time due to technical or time limitations.

CRediT authorship contribution statement

Anamika Singh: Conceptualization, Data curation, Formal analysis, Methodology, Validation, Visualization, Writing - original draft. **Alok Raghav:** Conceptualization, Data curation, Formal analysis, Methodology, Writing - original draft. **Parvaiz Ahmad Shiekh:** Formal analysis, Investigation, Visualization, Validation, Writing - review & editing. **Ashok Kumar:** Conceptualization, Funding acquisition, Investigation, Project administration, Resources, Software, Supervision, Validation, Writing - review & editing.

Declaration of competing interest

The authors declare that they have no known competing financial interests or personal relationships that could have appeared to influence the work reported in this paper.

Acknowledgment

The work was funded by the Department of Biotechnology (DBT) (#BT/PR13561/MED/32/392/2016 and #DBT/IN/SWEDEN/08/AK/2017-1); Department of Science and Technology (DST) (#DST/NM/NT-2018/48 and #DST/INT/SWD/P-11/2016); Ministry of Human Resource Development- IMPRINT (MHRD_6714/Healthcare), Ministry of Human Resource Development- SPARC (SPARC/2018–2019/P612/SL), and Ministry of Human Resource Development-UAY (MHRD_IITK_006), Govt. of India. AS and PAS would like to acknowledge IIT Kanpur for fellowship for the Ph.D. program. The authors would like to acknowledge Sophisticated Analytical Instrumentation Facility (SAIF), Council for Scientific and Industrial Research- Central Drug Research Institute, Lucknow for the LC-MS/MS analysis.

Abbreviations

T1DM	Type 1 diabetes mellitus
T2DM	Type 2 diabetes mellitus
BCA	bicinchoninic acid assay
BMSCs	bone marrow mesenchymal stromal cells
BSA	bovine serum albumin
CHEMS	Cholesteryl hemisuccinate
CMAP	compound muscle action potential
DCES	Designer conducting exosomal system
DLS	differential light scattering
DM	Diabetes mellitus
DMEM	Dulbecco's Modified Eagle Media
DPN	diabetic peripheral neuropathy
DPPC	1, 2-Dipalmitoyl-sn-glycero-3-phosphocholine
ERK	extracellular-signal-regulated kinase
ES	electrical stimulation
EVs	extracellular vesicles
Exo	exosomes
FBG	fasting blood glucose
FBS	fetal bovine serum
FE-SEM	Field emission scanning electron microscopy
TEM	transmission electron microscopy
FTIR	Fourier-transform infrared spectroscopy
GAPDH	Glyceraldehyde 3-phosphate dehydrogenase
GF	Grooming frequency
H&E	hematoxylin and eosin
MAG	myelin-associated glycoprotein
MBP	myelin basic protein
MNCV	motor nerve conduction velocity
MPZ	Myelin and protein zero
NCV	Nerve conduction velocity
OHDG	8-hydroxy-2' –deoxyguanosine
PCNA	proliferating cell nuclear antigen
PGK	phosphoglycerate kinase

PGM	phosphoglucomutase
PpyNps	polypyrrole nanoparticles
STZ	streptozotocin

Appendix A. Supplementary data

Supplementary data to this article can be found online at https://doi.org/10.1016/j.bioactmat.2021.01.008.
Supplementary video related to this article can be found at https://doi.org/10.1016/j.bioactmat.2021.01.008

References

[1] R. Pop-Busui, A.J.M. Boulton, E.L. Feldman, V. Bril, R. Freeman, R.A. Malik, J. M. Sosenko, D. Ziegler, Diabetic neuropathy: a position statement by the American diabetes association, Diabetes Care 40 (2017) 136–154, https://doi.org/10.2337/dc16-2042.

[2] S. Yagihashi, H. Mizukami, K. Sugimoto, Mechanism of diabetic neuropathy: where are we now and where to go? J. Diabetes Investig. 2 (2011) 18–32, https://doi.org/10.1111/j.2040-1124.2010.00070.x.

[3] S. Kambiz, J.W. van Neck, S.G. Cosgun, M.H.N. van Velzen, J.A.M.J.L. Janssen, N. Avazverdi, S.E.R. Hovius, E.T. Walbeehm, Correction: an early diagnostic tool for diabetic peripheral neuropathy in rats, PloS One 10 (2015), e0131144, https://doi.org/10.1371/journal.pone.0131144.

[4] A. Singh, P.A. Shiekh, M. Das, J. Seppälä, A. Kumar, Aligned chitosan-gelatin cryogel-filled polyurethane nerve guidance channel for neural tissue engineering: fabrication, characterization, and in vitro evaluation, Biomacromolecules 20 (2019) 662–673, https://doi.org/10.1021/acs.biomac.8b01308.

[5] A. Singh, S. Asikainen, A.K. Teotia, P.A. Shiekh, E. Huotilainen, I. Qayoom, J. Partanen, J. Seppälä, A. Kumar, Biomimetic photocurable three-dimensional printed nerve guidance channels with aligned cryomatrix lumen for peripheral nerve regeneration, ACS Appl. Mater. Interfaces 10 (2018) 43327–43342, https://doi.org/10.1021/acsami.8b11677.

[6] Y. Mukhamedshina, O. Gracheva, D. Mukhutdinova, Y. Chelyshev, A. Rizvanov, Mesenchymal stem cells and the neuronal microenvironment in the area of spinal cord injury, Neural Regen. Res. 14 (2019) 227, https://doi.org/10.4103/1673-5374.244778.

[7] Y.-H. Chang, K.-C. Wu, H.-J. Harn, S.-Z. Lin, D.-C. Ding, Exosomes and stem cells in degenerative disease diagnosis and therapy, Cell Transplant. 27 (2018) 349–363, https://doi.org/10.1177/0963689717723636.

[8] K.W. Witwer, B.W.M. Van Balkom, S. Bruno, A. Choo, M. Dominici, M. Gimona, A. F. Hill, D. De Kleijn, M. Koh, R.C. Lai, S.A. Mitsialis, L.A. Ortiz, E. Rohde, T. Asada, W.S. Toh, D.J. Weiss, L. Zheng, B. Giebel, S.K. Lim, Defining mesenchymal stromal cell (MSC)-derived small extracellular vesicles for therapeutic applications, J. Extracell. Vesicles 8 (2019) 1609206, https://doi.org/10.1080/20013078.2019.1609206.

[9] H. Jing, X. He, J. Zheng, Exosomes and regenerative medicine: state of the art and perspectives, Transl. Res. 196 (2018) 1–16, https://doi.org/10.1016/j.trsl.2018.01.005.

[10] R. Kalluri, V.S. LeBleu, The biology , function , and biomedical applications of exosomes, Science 367 (2020), eaau6977, https://doi.org/10.1126/science.aau6977, 80-.

[11] W.S. Toh, R.C. Lai, B. Zhang, S.K. Lim, MSC exosome works through a protein-based mechanism of action, Biochem. Soc. Trans. 46 (2018) 843–853, https://doi.org/10.1042/BST20180079.

[12] Q. Shi, Z. Qian, D. Liu, J. Sun, X. Wang, H. Liu, J. Xu, X. Guo, GMSC-derived exosomes combined with a chitosan/silk hydrogel sponge accelerates wound healing in a diabetic rat skin defect model, Front. Physiol. 8 (2017) 904, https://doi.org/10.3389/fphys.2017.00904.

[13] B. Mead, S. Tomarev, Bone marrow-derived mesenchymal stem cells-derived exosomes promote survival of retinal ganglion cells through miRNA-dependent mechanisms, Stem Cells Transl. Med. 6 (2017) 1273–1285, https://doi.org/10.1002/sctm.16-0428.

[14] T. Katsuda, T. Ochiya, Molecular signatures of mesenchymal stem cell-derived extracellular vesicle-mediated tissue repair, Stem Cell Res. Ther. 6 (2015) 212, https://doi.org/10.1186/s13287-015-0214-y.

[15] M. Ma, B. Li, M. Zhang, L. Zhou, F. Yang, F. Ma, H. Shao, Q. Li, X. Li, X. Zhang, Therapeutic effects of mesenchymal stem cell-derived exosomes on retinal detachment, Exp. Eye Res. 191 (2020) 107899, https://doi.org/10.1016/j.exer.2019.107899.

[16] K. Yin, S. Wang, R.C. Zhao, Exosomes from mesenchymal stem/stromal cells: a new therapeutic paradigm, Biomark. Res. 7 (2019) 8, https://doi.org/10.1186/s40364-019-0159-x.

[17] A. Damania, D. Jaiman, A.K. Teotia, A. Kumar, Mesenchymal stromal cell-derived exosome-rich fractionated secretome confers a hepatoprotective effect in liver injury, Stem Cell Res. Ther. 9 (2018) 31, https://doi.org/10.1186/s13287-017-0752-6.

[18] P.A. Shiekh, A. Singh, A. Kumar, Exosome laden oxygen releasing antioxidant and antibacterial cryogel wound dressing OxOBand alleviate diabetic and infectious wound healing, Biomaterials 249 (2020), https://doi.org/10.1016/j.biomaterials.2020.120020.

[19] X. Li, X. Xie, W. Lian, R. Shi, S. Han, H. Zhang, L. Lu, M. Li, Exosomes from adipose-derived stem cells overexpressing Nrf2 accelerate cutaneous wound healing by promoting vascularization in a diabetic foot ulcer rat model, Exp. Mol. Med. 50 (2018) 29, https://doi.org/10.1038/s12276-018-0058-5.

[20] S. Nojehdehi, S. Soudi, A. Hesampour, S. Rasouli, M. Soleimani, S.M. Hashemi, Immunomodulatory effects of mesenchymal stem cell–derived exosomes on experimental type-1 autoimmune diabetes, J. Cell. Biochem. 119 (2018) 9433–9443, https://doi.org/10.1002/jcb.27260.

[21] Y. Xiao, L. Zheng, X. Zou, J. Wang, J. Zhong, T. Zhong, Extracellular vesicles in type 2 diabetes mellitus: key roles in pathogenesis, complications, and therapy, J. Extracell. Vesicles 8 (2019) 1625677, https://doi.org/10.1080/20013078.2019.1625677.

[22] D. Sabry, S. Marzouk, R. Zakaria, H.A. Ibrahim, M. Samir, The effect of exosomes derived from mesenchymal stem cells in the treatment of induced type 1 diabetes mellitus in rats, Biotechnol. Lett. 42 (2020) 1597–1610, https://doi.org/10.1007/s10529-020-02908-y.

[23] Y. Sun, H. Shi, S. Yin, C. Ji, X. Zhang, B. Zhang, P. Wu, Y. Shi, F. Mao, Y. Yan, W. Xu, H. Qian, Human mesenchymal stem cell derived exosomes alleviate type 2 diabetes mellitus by reversing peripheral insulin resistance and relieving β-cell destruction, ACS Nano 12 (2018) 7613–7628, https://doi.org/10.1021/acsnano.7b07643.

[24] Y.-C. Lin, C.-H. Kao, C.-C. Chen, C.-J. Ke, C.-H. Yao, Y.-S. Chen, Time-course effect of electrical stimulation on nerve regeneration of diabetic rats, PloS One 10 (2015), e0116711, https://doi.org/10.1371/journal.pone.0116711.

[25] R. Dabby, M. Sadeh, I. Goldberg, V. Finkelshtein, Electrical stimulation of the posterior tibial nerve reduces neuropathic pain in patients with polyneuropathy, J. Pain Res. 10 (2017) 2717, https://doi.org/10.2147/JPR.S137420.

[26] G. Thakral, P.J. Kim, J. LaFontaine, R. Menzies, B. Najafi, L.A. Lavery, Electrical stimulation as an adjunctive treatment of painful and sensory diabetic neuropathy, J. Diabetes Sci. Technol. 7 (2013) 1202–1209, https://doi.org/10.1177/193229681300700510.

[27] B. Ferrigno, R. Bordett, N. Duraisamy, J. Moskow, M.R. Arul, S. Rudraiah, S. P. Nukavarapu, A.T. Vella, S.G. Kumbar, Bioactive polymeric materials and electrical stimulation strategies for musculoskeletal tissue repair and regeneration, Bioact. Mater. 5 (2020) 468–485, https://doi.org/10.1016/j.bioactmat.2020.03.010.

[28] J. Min, M. Patel, W.-G. Koh, J.H. Min, M. Patel, W.-G. Koh, Incorporation of conductive materials into hydrogels for tissue engineering applications, Polymers 10 (2018) 1078, https://doi.org/10.3390/polym10101078.

[29] R. Balint, N.J. Cassidy, S.H. Cartmell, Conductive polymers: towards a smart biomaterial for tissue engineering, Acta Biomater. 10 (2014) 2341–2353, https://doi.org/10.1016/J.ACTBIO.2014.02.015.

[30] T. Vishnoi, A. Kumar, Conducting cryogel scaffold as a potential biomaterial for cell stimulation and proliferation, J. Mater. Sci. Mater. Med. 24 (2013) 447–459, https://doi.org/10.1007/s10856-012-4795-z.

[31] T. Vishnoi, A. Singh, A.K. Teotia, A. Kumar, Chitosan-gelatin-polypyrrole cryogel matrix for stem cell differentiation into neural lineage and sciatic nerve regeneration in peripheral nerve injury model, ACS Biomater. Sci. Eng. 5 (2019) 3007–3021, https://doi.org/10.1021/acsbiomaterials.9b00242.

[32] J. Upadhyay, A. Kumar, B. Gogoi, A.K. Buragohain, Biocompatibility and antioxidant activity of polypyrrole nanotubes, Synth. Met. 189 (2014) 119–125, https://doi.org/10.1016/J.SYNTHMET.2014.01.004.

[33] L. Ghasemi-Mobarakeh, M.P. Prabhakaran, M. Morshed, M.H. Nasr-Esfahani, H. Baharvand, S. Kiani, S.S. Al-Deyab, S. Ramakrishna, Application of conductive polymers, scaffolds and electrical stimulation for nerve tissue engineering, J. Tissue Eng. Regen. Med. 5 (2011) e17–e35, https://doi.org/10.1002/term.383.

[34] J. Huang, L. Lu, J. Zhang, X. Hu, Y. Zhang, W. Liang, S. Wu, Z. Luo, Electrical stimulation to conductive scaffold promotes axonal regeneration and remyelination in a rat model of large nerve defect, PloS One 7 (2012), e39526, https://doi.org/10.1371/journal.pone.0039526.

[35] Y. Lin, J. Wu, W. Gu, Y. Huang, Z. Tong, L. Huang, J. Tan, Exosome-liposome hybrid nanoparticles deliver CRISPR/Cas9 system in MSCs, Adv. Sci. (Weinheim, Baden-Wurttemberg, Ger. 5 (2018) 1700611, https://doi.org/10.1002/advs.201700611.

[36] H.T. Nguyen, T.H. Tran, R.K. Thapa, C.D. Phung, B.S. Shin, J.-H. Jeong, H.-G. Choi, C.S. Yong, J.O. Kim, Targeted co-delivery of polypyrrole and rapamycin by trastuzumab-conjugated liposomes for combined chemo-photothermal therapy, Int. J. Pharm. 527 (2017) 61–71, https://doi.org/10.1016/j.ijpharm.2017.05.034.

[37] S. Dokka, D. Toledo, X. Shi, V. Castranova, Y. Rojanasakul, Oxygen radical-mediated pulmonary toxicity induced by some cationic liposomes, Pharm. Res. (N. Y.) 17 (2000) 521–525, https://doi.org/10.1023/A:1007504613351.

[38] L.F. Neves, J. Duan, A. Voelker, A. Khanal, L. McNally, J. Steinbach-Rankins, B. P. Ceresa, Preparation and optimisation of anionic liposomes for delivery of small

peptides and cDNA to human corneal epithelial cells, J. Microencapsul. 33 (2016) 391–399, https://doi.org/10.1080/02652048.2016.1202343.
[39] K.-D. Lee, S. Nirj, D. Papahadjopoulos, Quantitative analysis of liposome-cell interactions in vitro: rate constants of binding and endocytosis with suspension and adherent J774 cells and human monocytes 1. https://pubs.acs.org/sharinggguidelines, 1993 accessed November 5, 2020.
[40] K.D. Lee, K. Hong, D. Papahadjopoulos, Recognition of liposomes by cells: in vitro binding and endocytosis mediated by specific lipid headgroups and surface charge density, BBA - Biomembr 1103 (1992) 185–197, https://doi.org/10.1016/0005-2736(92)90086-2.
[41] A.M.R. Abbasi, M. Marsalkova, J. Militky, Conductometry and size characterization of polypyrrole nanoparticles produced by ball milling, J. Nanoparticles. (2013) 1–4, https://doi.org/10.1155/2013/690407, 2013.
[42] Y.T. Sato, K. Umezaki, S. Sawada, S. Mukai, Y. Sasaki, N. Harada, H. Shiku, K. Akiyoshi, Engineering hybrid exosomes by membrane fusion with liposomes, Sci. Rep. 6 (2016) 21933, https://doi.org/10.1038/srep21933.
[43] M. Piffoux, A.K.A. Silva, C. Wilhelm, F. Gazeau, D. Tareste, Modification of extracellular vesicles by fusion with liposomes for the design of personalized biogenic drug delivery systems, ACS Nano 12 (2018) 6830–6842, https://doi.org/10.1021/acsnano.8b02053.
[44] S. Ahmad, B. Gangaraj, H. Eisazadeh, E. Sadeghi, Preparation and characterization of polypyrrole nanocomposites by using various surfactants and Fe_2O_3 nanoparticles in aqueous media, J. Vinyl Addit. Technol. 22 (2016) 362–367, https://doi.org/10.1002/vnl.21449.
[45] S. Zhang, K. Zhu, G. Lv, G. Wang, D. Yu, J. Shao, UV-catalytic preparation of polypyrrole nanoparticles induced by H_2O_2, J. Phys. Chem. C 119 (2015) 18707–18718, https://doi.org/10.1021/acs.jpcc.5b03883.
[46] K.J. McKelvey, K.L. Powell, A.W. Ashton, J.M. Morris, S.A. McCracken, Exosomes: mechanisms of uptake, J. Circ. Biomarkers. 4 (2015) 7, https://doi.org/10.5772/61186.
[47] B.S. Joshi, M.A. de Beer, B.N.G. Giepmans, I.S. Zuhorn, Endocytosis of extracellular vesicles and release of their cargo from endosomes, ACS Nano 14 (2020) 4444–4455, https://doi.org/10.1021/acsnano.9b10033.
[48] A.M. Janas, K. Sapoń, T. Janas, M.H.B. Stowell, T. Janas, Exosomes and other extracellular vesicles in neural cells and neurodegenerative diseases, Biochim. Biophys. Acta Biomembr. 1858 (2016) 1139–1151, https://doi.org/10.1016/j.bbamem.2016.02.011.
[49] W.D. Gray, A.J. Mitchell, C.D. Searles, An accurate, precise method for general labeling of extracellular vesicles, Methods 2 (2015) 360–367, https://doi.org/10.1016/j.mex.2015.08.002.
[50] N. Hattangady, M. Rajadhyaksha, A brief review of in vitro models of diabetic neuropathy, Int. J. Diabetes Dev. Ctries. 29 (2009) 143, https://doi.org/10.4103/0973-3930.57344.
[51] T. Puig-Pijuan, M.A. de Godoy, L.R. Pinheiro Carvalho, V. Bodart-Santos, R. S. Lindoso, P.M. Pimentel-Coelho, R. Mendez-Otero, Human Wharton's jelly mesenchymal stem cells protect neural cells from oxidative stress through paracrine mechanisms, Futur. Sci. OA. (2020) FSO627, https://doi.org/10.2144/fsoa-2020-0036.
[52] M.A. de Godoy, L.M. Saraiva, L.R.P. de Carvalho, A. Vasconcelos-dos-Santos, H.J. V. Beiral, A.B. Ramos, L.R. de P. Silva, R.B. Leal, V.H.S. Monteiro, C.V. Braga, C. A. de Araujo-Silva, L.C. Sinis, V. Bodart-Santos, T.H. Kasai-Brunswick, C. de L. Alcantara, A.P.C.A. Lima, N.L. da Cunha-e Silva, A. Galina, A. Vieyra, F.G. De Felice, R. Mendez-Otero, S.T. Ferreira, Mesenchymal stem cells and cell-derived extracellular vesicles protect hippocampal neurons from oxidative stress and synapse damage induced by amyloid-β oligomers, J. Biol. Chem. 293 (2018) 1957–1975, https://doi.org/10.1074/jbc.M117.807180.
[53] L. Ko, T. Odawara, S.H. Yen, Menadione-induced tau dephosphorylation in cultured human neuroblastoma cells, Brain Res. 760 (1997) 118–128, https://doi.org/10.1016/s0006-8993(97)00292-8.
[54] J.Y. Zhou, Z. Zhang, G.S. Qian, Mesenchymal stem cells to treat diabetic neuropathy: a long and strenuous way from bench to the clinic, Cell Death Dis. 2 (2016) 16055, https://doi.org/10.1038/cddiscovery.2016.55.
[55] A. Akbari, N. Jabbari, R. Sharifi, M. Ahmadi, A. Vahhabi, S.J. Seyedzadeh, M. Nawaz, S. Szafert, M. Mahmoodi, E. Jabbari, R. Asghari, J. Rezaie, Free and hydrogel encapsulated exosome-based therapies in regenerative medicine, Life Sci. 249 (2020) 117447, https://doi.org/10.1016/j.lfs.2020.117447.
[56] R. Ren, X.H. Tan, J.H. Zhao, Q.P. Zhang, X.F. Zhang, Z.J. Ma, Y.N. Peng, Q.B. Liu, H.Y. Zhang, Y.Q. Li, R. He, Z.Q. Zhao, X.N. Yi, Bone marrow mesenchymal stem cell-derived exosome uptake and retrograde transport can occur at peripheral nerve endings, Artif. Cells, Nanomedicine Biotechnol 47 (2019) 2918–2929, https://doi.org/10.1080/21691401.2019.1640713.
[57] B. Fan, C. Li, A. Szalad, L. Wang, W. Pan, R. Zhang, M. Chopp, Z.G. Zhang, X.S. Liu, Mesenchymal stromal cell-derived exosomes ameliorate peripheral neuropathy in a mouse model of diabetes, Diabetologia 63 (2020) 431–443, https://doi.org/10.1007/s00125-019-05043-0.
[58] Y. Ma, S. Ge, J. Zhang, D. Zhou, L. Li, X. Wang, J. Su, Mesenchymal stem cell-derived extracellular vesicles promote nerve regeneration after sciatic nerve crush injury in rats, Int. J. Clin. Exp. Pathol. 10 (2017) 10032–10039. http://www.ncbi.nlm.nih.gov/pubmed/31966893. accessed December 1, 2020.
[59] J.L. Senger, K.M. Chan, H. Macandili, A.W.M. Chan, V.M.K. Verge, K.E. Jones, C. A. Webber, Conditioning electrical stimulation promotes functional nerve regeneration, Exp. Neurol. 315 (2019) 60–71, https://doi.org/10.1016/j.expneurol.2019.02.001.
[60] B.J. Kim, H.K. Jin, J.-S. Bae, Bone marrow-derived mesenchymal stem cells improve the functioning of neurotrophic factors in a mouse model of diabetic neuropathy, Lab. Anim. Res. 27 (2011) 171, https://doi.org/10.5625/lar.2011.27.2.171.
[61] B. Fan, C. Li, A. Szalad, L. Wang, W. Pan, R. Zhang, M. Chopp, Z.G. Zhang, X.S. Liu, Mesenchymal stromal cell-derived exosomes ameliorate peripheral neuropathy in a mouse model of diabetes, Diabetologia 63 (2020) 431–443, https://doi.org/10.1007/s00125-019-05043-0.
[62] B. Mead, S. Tomarev, Retinal ganglion cell neuroprotection by growth factors and exosomes: lessons from mesenchymal stem cells, Neural Regen. Res. 13 (2018) 228, https://doi.org/10.4103/1673-5374.226392.
[63] J. Chen, M. Chopp, Exosome therapy for stroke, Stroke 49 (2018) 1083–1090, https://doi.org/10.1161/STROKEAHA.117.018292.
[64] H. Xin, Y. Li, B. Buller, M. Katakowski, Y. Zhang, X. Wang, X. Shang, Z.G. Zhang, M. Chopp, Exosome-mediated transfer of miR-133b from multipotent mesenchymal stromal cells to neural cells contributes to neurite outgrowth, Stem Cell. 30 (2012) 1556–1564, https://doi.org/10.1002/stem.1129.
[65] Y. Zhang, M. Chopp, X.S. Liu, M. Katakowski, X. Wang, X. Tian, D. Wu, Z.G. Zhang, Exosomes derived from mesenchymal stromal cells promote axonal growth of cortical neurons, Mol. Neurobiol. 54 (2017) 2659–2673, https://doi.org/10.1007/s12035-016-9851-0.
[66] L. Qing, H. Chen, J. Tang, X. Jia, Exosomes and their MicroRNA cargo: new players in peripheral nerve regeneration, neurorehabil, Neural Repair 32 (2018) 765–776, https://doi.org/10.1177/1545968318798955.
[67] A.A. Al-Majed, T.M. Brushart, T. Gordon, Electrical stimulation accelerates and increases expression of BDNF and trkB mRNA in regenerating rat femoral motoneurons, Eur. J. Neurosci. 12 (2000) 4381–4390, https://doi.org/10.1111/j.1460-9568.2000.01341.x.
[68] N.E. Cameron, M.A. Cotter, S. Robertson, E.K. Maxfield, Nerve function in experimental diabetes in rats: effects of electrical stimulation, Am. J. Physiol. Metab. 264 (1993) E161–E166, https://doi.org/10.1152/ajpendo.1993.264.2.E161.
[69] Z.H. Serry, G. Mossa, H. Elhabashy, S. Elsayed, R. Elhadidy, R. Azmy, A. Mokhtar, Transcutaneous nerve stimulation versus aerobic exercise in diabetic neuropathy, Egypt, J. Neurol. Psychiatry Neurosurg. 53 (2016) 124, https://doi.org/10.4103/1110-1083.183449.
[70] H. Xu, J.M. Holzwarth, Y. Yan, P. Xu, H. Zheng, Y. Yin, S. Li, P.X. Ma, Conductive PPY/PDLLA conduit for peripheral nerve regeneration, Biomaterials 35 (2014) 225–235, https://doi.org/10.1016/j.biomaterials.2013.10.002.
[71] D. Jafari, S. Shajari, R. Jafari, N. Mardi, H. Gomari, F. Ganji, M. Forouzandeh Moghadam, A. Samadikuchaksaraei, Designer exosomes: a new platform for Biotechnology therapeutics, BioDrugs 34 (2020) 567–586, https://doi.org/10.1007/s40259-020-00434-x.
[72] L. Alvarez-Erviti, Y. Seow, H. Yin, C. Betts, S. Lakhal, M.J.A. Wood, Delivery of siRNA to the mouse brain by systemic injection of targeted exosomes, Nat. Biotechnol. 29 (2011) 341–345, https://doi.org/10.1038/nbt.1807.
[73] L. Cheng, K. Zhang, S. Wu, M. Cui, T. Xu, Focus on mesenchymal stem cell-derived exosomes: opportunities and challenges in cell-free therapy, Stem Cell. Int. (2017) 1–10, https://doi.org/10.1155/2017/6305295, 2017.
[74] M. Zafar, S. Naeem-ul-Hassan Naqvi, Effects of STZ-induced diabetes on the relative weights of kidney, liver and pancreas in albino rats: a comparative study, Int. J. Morphol. 28 (2010) 135–142, https://doi.org/10.4067/S0717-95022010000100019.
[75] F.C. Howarth, M. Jacobson, M. Shafiullah, E. Adeghate, Long-term effects of streptozotocin-induced diabetes on the electrocardiogram, physical activity and body temperature in rats, Exp. Physiol. 90 (2005) 827–835, https://doi.org/10.1113/expphysiol.2005.031252.
[76] C.Y. Liu, G. Yin, Y.D. Sun, Y.F. Lin, Z. Xie, A.W. English, Q.F. Li, H.D. Lin, Effect of exosomes from adipose-derived stem cells on the apoptosis of Schwann cells in peripheral nerve injury, CNS Neurosci. Ther. 26 (2020) 189–196, https://doi.org/10.1111/cns.13187.
[77] W.I. Sivitz, M.A. Yorek, Mitochondrial dysfunction in diabetes: from molecular mechanisms to functional significance and therapeutic opportunities, Antioxidants Redox Signal. 12 (2010) 537–577, https://doi.org/10.1089/ars.2009.2531.
[78] H. Yasuda, M. Terada, K. Maeda, S. Kogawa, M. Sanada, M. Haneda, A. Kashiwagi, R. Kikkawa, Diabetic neuropathy and nerve regeneration, Prog. Neurobiol. 69 (2003) 229–285, https://doi.org/10.1016/s0301-0082(03)00034-0.
[79] D. Frohlich, W.P. Kuo, C. Fruhbeis, J.-J. Sun, C.M. Zehendner, H.J. Luhmann, S. Pinto, J. Toedling, J. Trotter, E.-M. Kramer-Albers, Multifaceted effects of oligodendroglial exosomes on neurons: impact on neuronal firing rate, signal transduction and gene regulation, Philos. Trans. R. Soc. B Biol. Sci. 369 (2014), https://doi.org/10.1098/rstb.2013.0510, 20130510–20130510.
[80] F. Arslan, R.C. Lai, M.B. Smeets, L. Akeroyd, A. Choo, E.N.E. Aguor, L. Timmers, H. V van Rijen, P.A. Doevendans, G. Pasterkamp, S.K. Lim, D.P. de Kleijn, Mesenchymal stem cell-derived exosomes increase ATP levels, decrease oxidative stress and activate PI3K/Akt pathway to enhance myocardial viability and prevent adverse remodeling after myocardial ischemia/reperfusion injury, Stem Cell Res. 10 (2013) 301–312, https://doi.org/10.1016/j.scr.2013.01.002.
[81] L. Cheng, K. Zhang, S. Wu, M. Cui, T. Xu, Focus on mesenchymal stem cell-derived exosomes: opportunities and challenges in cell-free therapy, Stem Cell. Int. (2017) 1–10, https://doi.org/10.1155/2017/6305295, 2017.
[82] J.W. Han, D. Choi, M.Y. Lee, Y.H. Huh, Y.S. Yoon, Bone marrow-derived mesenchymal stem cells improve diabetic neuropathy by direct modulation of both angiogenesis and myelination in peripheral nerves, Cell Transplant. 25 (2016) 313–326, https://doi.org/10.3727/096368915X688209.
[83] S.P. Frostick, Q. Yin, G.J. Kemp, Schwann cells, neurotrophic factors, and peripheral nerve regeneration, Microsurgery 18 (1998) 397–405, https://doi.org/10.1002/(SICI)1098-2752(1998)18:7<397::AID-MICR2>3.0.CO;2-F.

[84] K.S. Rachana, M.S. Manu, G.M. Advirao, Insulin influenced expression of myelin proteins in diabetic peripheral neuropathy, Neurosci. Lett. 629 (2016) 110–115, https://doi.org/10.1016/j.neulet.2016.06.067.
[85] S.S. Reddy, K. Shruthi, D. Joy, G.B. Reddy, 4-PBA prevents diabetic muscle atrophy in rats by modulating ER stress response and ubiquitin-proteasome system, Chem. Biol. Interact. 306 (2019) 70–77, https://doi.org/10.1016/j.cbi.2019.04.009.
[86] Y.T. Tseng, W.H. Chang, C.C. Lin, F.R. Chang, P.C. Wu, Y.C. Lo, Protective effects of Liuwei dihuang water extracts on diabetic muscle atrophy, Phytomedicine 53 (2019) 96–106, https://doi.org/10.1016/j.phymed.2018.09.032.
[87] M.L. Dirks, B.T. Wall, T. Snijders, C.L.P. Ottenbros, L.B. Verdijk, L.J.C. Van Loon, Neuromuscular electrical stimulation prevents muscle disuse atrophy during leg immobilization in humans, Acta Physiol. 210 (2014) 628–641, https://doi.org/10.1111/apha.12200.
[88] M. Tanaka, T. Morifuji, M. Yoshikawa, R. Nakanishi, H. Fujino, Effects of combined treatment with blood flow restriction and low-intensity electrical stimulation on diabetes mellitus-associated muscle atrophy in rats, J. Diabetes 11 (2019) 326–334, https://doi.org/10.1111/1753-0407.12857.
[89] H. Yin, F. Price, M.A. Rudnicki, Satellite cells and the muscle stem cell niche, Physiol. Rev. 93 (2013) 23–67, https://doi.org/10.1152/physrev.00043.2011.
[90] R. Wu, C. Huang, Q. Wu, X. Jia, M. Liu, Z. Xue, Y. Qiu, X. Niu, Y. Wang, Exosomes secreted by urine-derived stem cells improve stress urinary incontinence by promoting repair of pubococcygeus muscle injury in rats, Stem Cell Res. Ther. 10 (2019) 80, https://doi.org/10.1186/s13287-019-1182-4.
[91] T. Yaman, A. Uyar, I. Celik, E.E. Alkan, O.F. Keles, Z. Yener, Histopathological and immunohistochemical study of antidiabetic effects of Heracleum persicum extract ın experimentally diabetic rats, Indian J. Pharm. Educ. Res. 51 (2017) S450–S457, https://doi.org/10.5530/ijper.51.3s.66.
[92] Q. Ge, X.X. Xie, X. Xiao, X. Li, Exosome-like vesicles as new mediators and therapeutic targets for treating insulin resistance and β -cell mass failure in type 2 diabetes mellitus, J. Diabetes Res. (2019) 1–7, https://doi.org/10.1155/2019/3256060, 2019.
[93] Y. Zhou, H. Xu, W. Xu, B. Wang, H. Wu, Y. Tao, B. Zhang, M. Wang, F. Mao, Y. Yan, S. Gao, H. Gu, W. Zhu, H. Qian, Exosomes released by human umbilical cord mesenchymal stem cells protect against cisplatin-induced renal oxidative stress and apoptosis in vivo and in vitro, Stem Cell Res. Ther. 4 (2013) 34, https://doi.org/10.1186/scrt194.
[94] A. Dorronsoro, P.D. Robbins, Regenerating the injured kidney with human umbilical cord mesenchymal stem cell-derived exosomes, Stem Cell Res. Ther. 42 (4) (2013) 39, https://doi.org/10.1186/scrt187, 2013.
[95] T. Shibata, K. Naruse, H. Kamiya, M. Kozakae, M. Kondo, Y. Yasuda, N. Nakamura, K. Ota, T. Tosaki, T. Matsuki, E. Nakashima, Y. Hamada, Y. Oiso, J. Nakamura, Transplantation of bone marrow-derived mesenchymal stem cells improves diabetic polyneuropathy in rats, Diabetes 57 (2008) 3099–3107, https://doi.org/10.2337/db08-0031.
[96] M.C. Lu, C.C. Tsai, S.C. Chen, F.J. Tsai, C.H. Yao, Y.S. Chen, Use of electrical stimulation at different current levels to promote recovery after peripheral nerve injury in rats, J. Trauma Inj. Infect. Crit. Care 67 (2009) 1066–1072, https://doi.org/10.1097/TA.0b013e318182351a.
[97] M. Shabani, M.H. Larizadeh, S. Parsania, V. Hajali, A. Shojaei, Evaluation of destructive effects of exposure to cisplatin during developmental stage: No profound evidence for sex differences in impaired motor and memory performance, Int. J. Neurosci. 122 (2012) 439–448, https://doi.org/10.3109/00207454.2012.673515.